AD-A127 042   AURORAL-REGION DYNAMICS DETERMINED WITH THE CHATANIKA   1/1
              RADAR(U) SRI INTERNATIONAL MENLO PARK CA V B WICKWAR
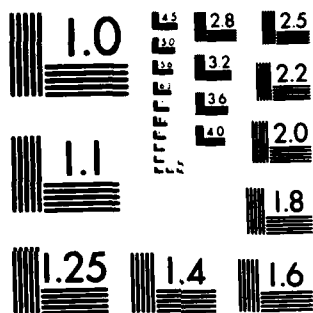   NOV 82 AFOSR-TR-83-0237 F49620-78-C-0018
UNCLASSIFIED   F/G 4/1   NL

END
DATE
FILMED
5-83
DTIC

AFOSR-TR- 83 - 0 2 3 7

Final Scientific Report   *November 1982*

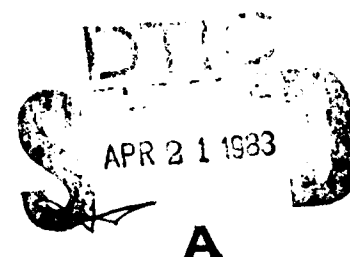# AURORAL-REGION DYNAMICS DETERMINED WITH THE CHATANIKA RADAR

By: VINCENT B. WICKWAR

333 Ravenswood Avenue
Menlo Park, California 94025 U.S.A.
(415) 326-6200
Cable: SRI INTL MPK
TWX: 910-373-2046

SRI International

Final Scientific Report   *November 1982*

AURORAL-REGION DYNAMICS DETERMINED WITH THE CHATANIKA RADAR

By: VINCENT B. WICKWAR

⋯ CH (AFSC)

⋯

Chief, ⋯ Information Division

Approved by:

ROBERT S. LEONARD, *Director*
Radio Physics Laboratory

DAVID D. ELLIOTT, *Vice President*
Research and Analysis Division

SECURITY CLASSIFICATION OF THIS PAGE (When Data Entered)

REPORT DOCUMENTATION PAGE	READ INSTRUCTIONS BEFORE COMPLETING FORM

1. REPORT NUMBER AFOSR-TR- 83-0237	2. GOVT ACCESSION NO. AD-A127042	3. RECIPIENT'S CATALOG NUMBER

4. TITLE (and Subtitle) AURORAL-REGION DYNAMICS DETERMINED WITH THE CHATANIKA RADAR	5. TYPE OF REPORT & PERIOD COVERED Final Scientific Report
	6. PERFORMING ORG. REPORT NUMBER

7. AUTHOR(s) Vincent B. Wickwar	8. CONTRACT OR GRANT NUMBER(s) Contract F49620-78-C-0018

9. PERFORMING ORGANIZATION NAME AND ADDRESS SRI International 333 Ravenswood Avenue Menlo Park, California 94025	10. PROGRAM ELEMENT, PROJECT, TASK AREA & WORK UNIT NUMBERS 61102F 2310/A2

11. CONTROLLING OFFICE NAME AND ADDRESS Department of the Air Force Air Force Office of Scientific Research (AFSC)/NC Bolling AFB, Washington, D.C. 20332	12. REPORT DATE November 1982	13. NO. OF PAGES 85
14. MONITORING AGENCY NAME & ADDRESS (if diff. from Controlling Office)	15. SECURITY CLASS. (of this report) UNCLASSIFIED	
	15a. DECLASSIFICATION/DOWNGRADING SCHEDULE	

16. DISTRIBUTION STATEMENT (of this report)

Approved for public release; distribution unlimited.

17. DISTRIBUTION STATEMENT (of the abstract entered in Block 20, if different from report)

18. SUPPLEMENTARY NOTES

19. KEY WORDS (Continue on reverse side if necessary and identify by block number)

Thermospheric winds	Incoherent-scatter radar
Gravity waves	Fabry-Perot interferometer
Auroral region	
Chatanika Radar	

20. ABSTRACT (Continue on reverse side if necessary and identify by block number)

An extensive body of data from the Chatanika Incoherent Scatter Radar was acquired between 1971 and 1978, and has been analyzed to learn about the winds in the upper atmosphere in the auroral region. These data have been supplemented by a body of correlative optical data from the Fabry-Perot interferometer operated by the Michigan Auroral Observatory. Most of these data pertain to winds in the lower F region between 180 and 200 km. The wind in the magnetic meridian has been examined, and for the first time, the radar and optical techniques have been compared. Good agreement was found for averaged and for

DD FORM 1473
1 JAN 73
EDITION OF 1 NOV 65 IS OBSOLETE

SECURITY CLASSIFICATION OF THIS PAGE (When Data Entered)

19. KEY WORDS (Continued)

20 ABSTRACT (Continued)

simultaneous observations. When averaged for 24 hours, a large net equatorward wind is found. During the night, this wind increases with magnetic activity. Because few summer and winter observations exist, seasonal variations cannot be derived. But the existing observations differ from those made at the equinoxes in the manner predicted by theory.

The radar data often showed very distinct large fluctuations superimposed on the slowly varying meridional wind. They occur night and day--usually as a single impulse, but once as a wave train. The periods range from 30 min to 2 hours. The fluctuations appear at the three altitudes examined--170, 225, and 280 km-- and usually grow with altitude, particularly between the first and second altitudes. In that sense, they behave like gravity waves. If they arise from variations in the horizontal neutral wind, the magnitude in the upper two altitudes is 200 to 400 m/s. However, simultaneous data from the Fabry-Perot on one night and independent data on other nights suggest that these disturbances are caused by variations in the vertical wind. In that case, the magnitude of the deduced radar disturbance is 50 to 100 m/s, in agreement with the Fabry-Perot findings. These large disturbances deserve future study.

On an additional eight nights, the zonal neutral wind was examined with the Fabry-Perot and the zonal ion velocity with the radar. The neutral wind was highly variable. On some occasions, it behaved as expected from solar EUV heating of the thermosphere. On others, it clearly responded to ion drag, and, on one occasion, the influence of Joule heating could be discerned.

At lower altitudes, in the lower thermosphere or E region between 90 and 140 km, another body of radar data is required, as well as a more involved data analysis procedure to examine the winds. Earlier results, before the complete analysis procedure was implemented, have indicated that these new data hold considerable promise.

CONTENTS

ILLUSTRATIONS

TABLES

ix

ACKNOWLEDGMENTS

I INTRODUCTION

In this report, we review the work that we have done to learn about
auroral region dynamics. The motivating factors behind this work are two:
scientific and technical. First, the simple picture of the dynamics of the
neutral atmosphere involves atmospheric heating by solar UV and EUV
radiation. This heating creates tides with periods of 24 hours and harmonics
thereof. Major perturbations to this picture originate in the auroral
region because of the transfer of energy and momentum from the magneto-
sphere to the ionosphere and atmosphere. This transfer involves Joule
and particle heating, and convection electric fields. Some of the effects
are transient, such as enhanced meridional and zonal winds, and gravity
waves; others are regular, such as enhanced net meridional flow and seasonal
variation. Second, the Chatanika Incoherent-Scatter Radar, a very powerful
tool for examining these effects, has been in operation in the auroral
region since July 1971. The scattered radio waves provide information
directly about the ionized portion of the medium, and well-established
physical relationships enable us to gain much information about the neutral
portion. In addition to the extensive body of radar data, a small set of
simultaneous optical data exists obtained with the Michigan Auroral Obser-
vatory (MAO) Fabry-Perot interferometer operated by John W. Meriwether, Jr.
This instrument is directly sensitive to the motion of the neutrals. The
comparison of these two data sets has proved particularly valuable to our
understanding of the neutral dynamics.

Because of the measurement technique, the study of the auroral region
dynamics divides into four areas that we discuss separately. In the
remainder of this section, we introduce these four areas indicating their
pertinent features and in general terms the questions we address. In
Section II, we discuss the measurement techniques and analyses. In
Section III, we discuss the comparison of winds derived from the radar
and Fabry-Perot interferometer. In the four subsequent sections, we discuss

1

our research work in each of the four areas and indicate what more we believe can be accomplished. In Section VIII, we give a summary.

A.   F-Region Meridional Wind

From a combination of experimental measurements of winds and atmospheric composition and of theoretical studies of solar energy deposition with resultant pressure bulges and winds, a model has emerged of large-scale circulation cells [Dickinson et al., 1981, and references therein]. The air in these cells rises in the auroral regions, flows towards mid- and low-latitudes, subsides there, and then flows back at lower altitudes. The equatorward or meridional flow occurs at F-region altitudes at fairly high velocities; the return flow at E-region altitudes occurs at much slower velocities because of the greater densities. This meridional wind varies with magnetic activity and with season. A schematic representation of the F-region component is shown in Figure 1.
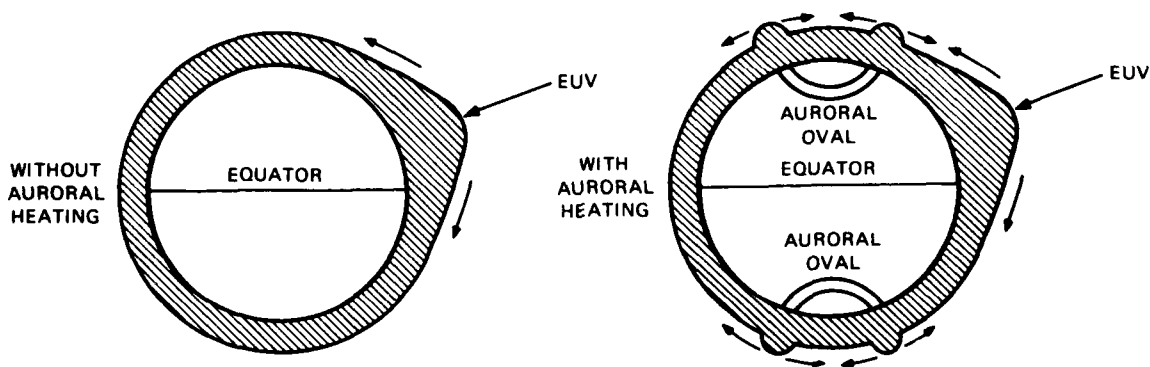
FIGURE 1   SCHEMATIC REPRESENTATION OF THE UPPER THERMOSPHERE SHOWING THE EFFECT OF EUV AND UV HEATING AS WELL AS PARTICLE AND JOULE HEATING IN THE AURORAL REGIONS

2

With the radar, we are able to observe the F-region meridional wind for the first time on a regular basis in the auroral region; furthermore, we can observe it for periods as long as 24 hours. With the Fabry-Perot, we can observe this component of the wind during the night. The simultaneous data from the two instruments provide the first opportunity to compare two independent measurements of the wind. This comparison is particularly valuable in the auroral zone for examining the assumptions inherent to each technique. Thus, the first step in the analysis is to compare results from the two independent techniques to determine whether or not they support each other. The next step is to establish the meridional-wind pattern in the auroral region and its variation with magnetic activity and with season. After establishing the pattern of variation, we, then, can examine the factors that control the variation.

B. F-Region Vertical Velocities and Gravity Waves

Many TIDs and gravity waves observed at mid- and low-latitudes originate in the auroral region [Davis and Da Rosa, 1969; Testud, 1970; Chandra et al., 1979]. They may be generated by particle precipitation, auroral electrojet currents, or Joule heating. They also may carry large amounts of energy to lower latitudes. We, therefore, would like to identify them in the source region. From the data set of simultaneous radar and Fabry-Perot data, we found a transient phenomenon involving large vertical neutral velocities that is most likely related to a large-scale or medium-scale gravity wave. The vertical velocities are of the magnitude predicted by Richmond and Matsushita [1975] and confirm the findings from the AE-C satellite of Spencer et al. [1976]. Since the initial identification, this phenomenon can be identified in the radar data alone. The first step in the analysis is to establish the nature of the phenomenon and to determine if it can be closely related to gravity waves. In the future particular experiments should be designed to confirm this finding and learn more about the pattern of occurrence and origin.

C.   F-Region Zonal Wind

In the auroral region, westward or eastward ion velocities can be
very large because of magnetospheric convection. These large ion velo-
cities, coupled with large F-region ion densities, produce an unusual
situation in the auroral region whereby the ions can impart significant
momentum to the neutrals, thus affecting their velocity. Likewise, strong
Joule heating is present in the auroral region. The question of which
process is the more important arises. From a unique data set of simultaneous
radar and Fabry-Perot measurements, we can examine the contributions to the
zonal wind. In this case, the radar is used to measure the ion velocities,
and the Fabry-Perot neutral velocities.

D.   E-Region Neutral Wind

In the E region, the basic wind pattern is tidal, resulting from the
absorption of solar EUV and UV radiation [Evans, 1978; Forbes and Garrett,
1979]. The tides have been studied at lower latitudes, but have received
little attention at high latitudes. This basic tidal pattern is most
likely strongly perturbed during magnetic storms and substorms. The
establishment of the existence of such perturbations is important because
of the implications for the transport of neutral constituents and because
of the possible feedback effect of the winds on the aurora itself. This
latter effect occurs because the electric field that is important for
currents to close in the ionosphere is itself a function of the neutral
wind [Evans et al., 1977]. Progress in this area has been in developing
the data-reduction procedures needed to obtain high-quality data on the
E-region horizontal neutral wind.

4

II TECHNIQUE

The incoherent-scatter radar technique is the principal measurement technique used in this study. A powerful radio signal is transmitted and scattered by electrons, whose motions are closely controlled by the ions. The received signal can, then, be analyzed for the density or concentration of electrons, the velocity of the ions, and the electron and ion temperatures. Using these quantities and the equations of motion for the ions and electrons, we can, then, deduce the neutral meridional wind in the F region and the vector neutral wind in the lower E region.

For the correlative optical observations, we used a Fabry-Perot interferometer to measure the emission spectrum from atomic oxygen near 630 nm. The Doppler shift of that spectrum gives the line-of-sight neutral wind in the lower F region. Several such line-of-sight winds are used to determine the vector wind.

In the remainder of this section, we explain in more detail the technical aspects of the neutral-wind measurements made with the radar and Fabry-Perot interferometer.

A.   Radar Measurements

The received radar signal has three important properties. From the total power, we learn about the electron density. From the Doppler shift, we determine the line-of-sight ion velocity. From the shape of the spectrum, we determine several factors depending on the altitude: (1) in the F region above 250 km, we determine the electron and ion temperatures; (2) in the E region between 110 and 140 km, we also determine the electron and ion temperatures; (3) when we supplement the measurements between 140 and 250 km with additional physical information, we may determine the ion mass in addition to the electron and ion temperatures [Kelly and Wickwar, 1981]; and (4) similarly, below 110 km, we infer the neutral density in addition to the electron and ion temperatures [Wickwar et al., 1981].

5

In principle, we can measure these three properties of the received radar signal simultaneously at all altitudes between 85 and 550 km. In practice, the power information has always been measured over the full altitude range. Our ability to measure the spectral information, however, has improved with time. Initially, the measurements were most appropriate to the region above 200 km, although they could be used down to 160 km. The capability to examine the region between 120 and 200 km was then added. Most recently, the region between 90 and 120 km was added. Now, we can measure the high-altitude region simultaneously with either one of the lower-altitude regions.

The ion velocities measured are in the direction of the radar line-of-sight. Because the radar is fully steerable, the measurements can be made in any desired direction, such as along the magnetic field line or in three or more directions. Examples of possible antenna pointing sequences are shown in Figure 2. Line-of-sight velocities suffice for some studies, but for others several such velocities are combined to obtain vector velocities.

1.   F-Region Meridional Wind

Above about 150 km, the ion-gyro frequency, Ω_i, is much greater than the ion-neutral collision frequency, ν_i, with the effect that the steady-state equations of motion for the electrons and ions become

(for ions and electrons)

$$\vec{E}_{\perp} + \vec{V}_{\perp} \times \vec{B} = 0, \qquad (1)$$

$$n_i m_i \nu_i (U_{11} - V_{11}) - \sin I \left(\frac{\partial P_i}{\partial h} + n_i m_i g \right) + n_i e E_{11} = 0, \qquad (2)$$

and

$$n_e m_e \nu_e (U_{11} - V_{e11}) - \sin I \left(\frac{\partial P_e}{\partial h} + n_e m_e g \right) - n_e e E_{11} = 0, \qquad (3)$$

6
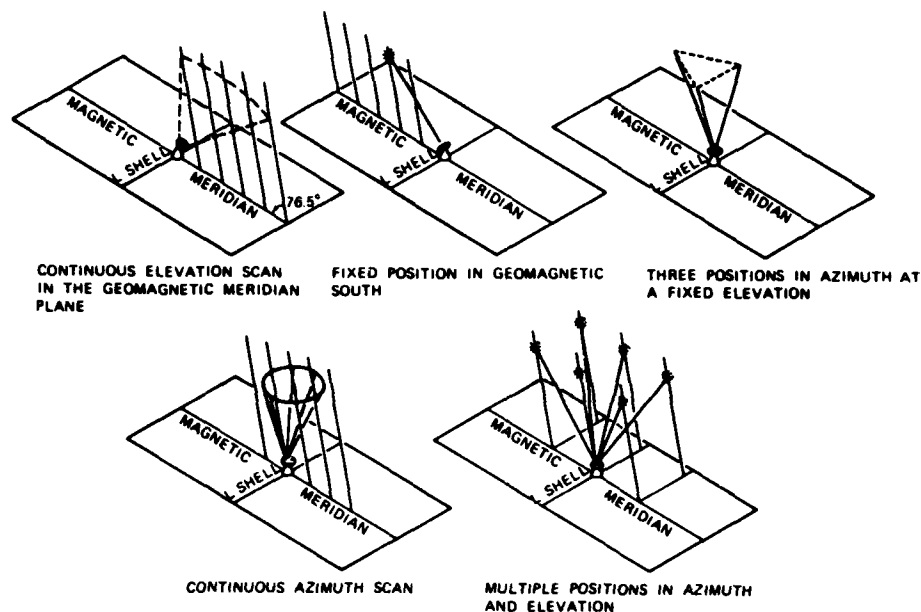
FIGURE 2   EXAMPLES OF SEQUENCES OF ANTENNA POSITIONS USED FOR RADAR
OBSERVATIONS. Most of these data were observed with the antenna in a fixed
position parallel to the magnetic field or in a sequence of three azimuths at fixed
elevation with one position parallel to the magnetic field.

where

$\vec{E}_\perp$ = Applied electric field perpendicular to B

E_{11} = Polarization electrostatic field

$\vec{B}$ = Magnetic field

I = Magnetic field inclination or dip angle
(~76.5° at Chatanika)

U_{11} = Neutral wind parallel to the magnetic field
and positive away from the earth

$\vec{V} = \vec{V}_\perp + V_{11}$ = Velocity of ions of species i. V_{11} is positive
away from earth

$V_e = \vec{V}_{e_\perp} + V_{e11}$ = Electron velocity

$P_i = n_i k T_i$ = Partial pressure of ions of species i

$P_e = n_e k T_e$ = Partial pressure of the electrons

n_i, m_i, T_i = Concentration, mass, and temperature of ions
of species i

n_e, m_e, T_e = Concentration, mass, and temperature of the electrons

7

$$\nu_i = \sum_n \nu_{in} = \text{Total ion-neutral collision frequency for ions of species } i$$

$$\nu_e = \sum_n \nu_{en} = \text{Total electron-neutral collision frequency.}$$

Examination of these equations shows that the neutral wind does not effect the ion velocity perpendicular to the magnetic field, but does effect the ion motion parallel to the magnetic field. When we solve Eqs. (2) and (3) for the polarization electric field and drop terms of the order of m_e/m_i, we obtain

$$V_{11} = U_{11} - \frac{kT_i}{m_i \nu_i} \sin I \left\{ \frac{1}{T_i} \frac{\partial(T_i + T_e)}{\partial h} + \frac{1}{n_i} \frac{\partial n_i}{\partial h} + \frac{T_e}{T_i} \frac{1}{n_e} \frac{\partial n_e}{\partial h} + \frac{m_i g}{kT_i} \right\} . \quad (4a)$$

For a major ion, such that $n_i \approx n_e$, this equation becomes

$$V_{11} = U_{11} - D \sin I \left\{ \frac{1}{T_p} \frac{\partial T_p}{\partial h} + \frac{1}{n_e} \frac{\partial n_e}{\partial h} + \frac{m_i g}{2kT_p} \right\}$$

$$\quad (4b)$$

$$= U_{11} - V_D \sin I$$

where

$$T_p = \frac{T_i + T_e}{2} = \text{Plasma temperature}$$

$$D = \frac{2kT_p}{m_i \nu_i} = \text{Ion-neutral diffusion coefficient}$$

$$V_D = \text{Ion-neutral diffusion velocity for ions of species } i.$$

Physcially, Eq. (4b) states that the motion of the major ion species parallel to the magnetic field is controlled by collisions with neutrals, pressure gradients arising from gradients in temperature and concentration, and gravity. Its application above 250 km is straightforward because O^+ is the dominant ion species and m_i and ν_i can be replaced by m_{0+} and ν_{0+}. Similarly, the ion velocity measured by the radar is that of O^+.

8

However, between 150 and 250 km, the situation is not as clear because there is a mixture of mostly O_2^+, NO^+ and O^+ ions. The question arises whether these ions have different diffusion velocities and how they affect the radar measurements. First, the O_2^+ ions can be discounted in favor of the NO^+ ions. Usually, the NO^+ concentration is far greater than the O_2^+ concentration [Swider and Narcissi, 1977]; additionally, the normalized gradients [Swider and Narcissi, 1977], masses, and ion-neutral collision frequencies [Schunk and Walker, 1973] are nearly the same. Second, we must examine the difference in ion-diffusion velocities for NO^+ and O^+. Let us define

$$q = \frac{[O^+]}{n_e}$$

$$p = \frac{[NO^+]}{n_e} \tag{5}$$

$$p + q = 1 \quad .$$

Equation (4a) then becomes

$$V_{11} = U_{11} - D_{O^+}\sin I \left\{ \frac{1}{T_p} \frac{\partial T_p}{\partial h} + \frac{1}{n_e} \frac{\partial n_e}{\partial h} + \frac{m_{O^+}g}{2kT_p} + \frac{T_i}{2T_p} \frac{1}{q} \frac{\partial q}{\partial h} \right\} \tag{4c}$$

for O^+ and

$$V_{11} = U_{11} - D_{NO^+}\sin I \left\{ \frac{1}{T_p} \frac{\partial T_p}{\partial h} + \frac{1}{n_e} \frac{\partial n_e}{\partial h} + \frac{m_{NO^+}g}{2kT_p} - \frac{T_i}{2T_p} \frac{1}{1-q} \frac{\partial q}{\partial h} \right\} \tag{4d}$$

for NO^+. For reasonable composition gradients, the difference in ion-diffusion velocities is less than 5 m/s. Because this difference is small, we make the simplifying assumption that the one ion velocity found from the Doppler shift of the radar signal is

$$V_{11} = U_{11} - \langle V_D \rangle \sin I \tag{6}$$

9

where

$$\langle V_D \rangle = q\, V_{O^+} + p\, V_{NO^+}$$

(7)

$$= \frac{2kT_p}{\langle m_i \nu_i \rangle} \left[\frac{1}{T_p} \frac{\partial T_p}{\partial h} + \frac{1}{n_e} \frac{\partial n_e}{\partial h} \right] + g \frac{\langle m_i \rangle}{\langle m_i \nu_i \rangle} \quad .$$

If the difference in diffusion velocities were large, we would have to be more careful in considering the radar signal because it is not a linear superposition of the signals scattered from the two ion species.

In the analysis program, we further simplify by replacing $\langle m_i \nu_i \rangle$ by $\langle m_i \rangle \langle \nu_i \rangle$. This simplification has no significant effect because the ion-neutral diffusion velocity is itself very small compared to the uncertainty in V_{11} in this altitude region where there is a mixture of ions.

If we can assume that the neutral motion is horizontal, as we are led to believe by the very small vertical velocities derived by Hays et al. [1973] for the worst cast of localized intense heating, then

$$U_{11} = -U_{MERID} \cos I$$

(8)

and the horizontal neutral wind in the magnetic meridian is given by

$$U_{MERID} = -\frac{V_{11}}{\cos I} - \frac{2kT_p}{\langle m_i \nu_i \rangle} \tan I \left\{ \frac{1}{T_p} \frac{\partial T_p}{\partial h} + \frac{1}{n_e} \frac{\partial n_e}{\partial h} + \frac{\langle m_i \rangle g}{2kT_p} \right\} \quad .$$

(9)

The sign convention adopted is that U_{MERID} is positive to the north.

In Eq. (9), V_{11} and $(1/n_e)(\partial n_e/\partial h)$ are obtained from the radar measurements. The other terms involving the ion composition, $\langle m_i \rangle$, $\langle m_i \nu_i \rangle$, $\langle \nu_i \rangle$, T_p, and $(1/T_p)(\partial T_p/\partial h)$ are obtained from models. These models have been chosen to approximate much of the radar data. The neutral atmosphere used to calculate the ν_i and the temperatures is the $1000°K$ atmosphere of Banks and Kockarts [1973], with the assumption that $T_e = 2T_i = 2T_n$. The ion composition is considered 75-percent NO^+ and

10

and 25-percent O_2^+ below 150 km, entirely O^+ above 250 km, and a linearly varying mixture in between the two altitudes.

The use of model quantities to calculate parts of the diffusion velocity in Eq. (9) has a greater impact on the uncertainty than the assumption previously introduced to obtain Eq. (7). Yet, detailed calculations of the ion-neutral diffusion velocity further show that, under most circumstances, the term is negligible below about 225 km, compared to the uncertainty in the measured V_{11}. At higher altitudes, the values assumed for the temperatures and for the ν_{O^+} become increasingly important, it may be possible to use the radar measurements of temperatures and the total ion-neutral collision frequency to improve on the diffusion calculation and deduce meridional winds at higher altitudes. Alternatively, if chemical release or satellite measurements were to show that no gradient in U_{MERID} existed above some altitude, then we could find the variation of ν_{O^+} (or of atomic oxygen) with altitude.

For the F-region meridional-wind determinations, we have restricted the data experiments to the radar line of sight along the magnetic field. In this way, V_{11} could be measured directly. This choice reduces the possibility of false V_{11} values that arise from temporal and spatial variations that occur when it is necessary to resolve three line-of-sight velocities. For much of the data set, the measurements were made continuously in that direction, giving a continuous time history of V_{11} and U_{11} with a possibility of time resolution between 2 and 10 min. For part of the data set, line-of-sight velocities were measured in three directions, one of which was along the magnetic field.

2.   F-Region Vertical Wind

In the previous section, in deriving U_{MERID}, Eq. (9), we assumed that the only significant neutral motion was horizontal. However, as we discuss in Section V, there do appear to be limited periods when the neutral wind has a strong vertical component. These vertical winds are much larger than those calculated by Hays et al. [1973].

11

Under these conditions

$$U_{11} = -U_{MERID} \cos I + U_{VERT} \sin I \qquad (10)$$

where we can determine the U_{MERID} component by interpolating between values on either side of the event, and where U_{VERT} is positive upward. From Eqs. (6) and (7), we then obtain

$$U_{VERT} = \frac{V_{11}}{\sin I} + \frac{2kT_p}{\langle m_i \nu_i \rangle} \left\{ \frac{1}{T_p} \frac{\partial T_p}{\partial h} + \frac{1}{n_e} \frac{\partial n_e}{\partial h} + \frac{\langle m_i \rangle g}{2kT_p} \right\} + \frac{U_{MERID}}{\tan I} \quad . \qquad (11)$$

Alternatively, if the data were initially interpreted as though there were only a meridional wind, U'_{MERID}, and if the meridional component were later determined to be U_{MERID}, then,

$$U_{VERT} = \frac{-\left(U'_{MERID} - U_{MERID}\right)}{\tan I} \quad . \qquad (12)$$

3. E-Region Neutral Winds

The important difference between the E and F regions for the equations of motion is that the ion-neutral collision frequency, ν_i, approaches and surpasses the ion-gyro frequency, Ω_i. The equation of motion for ions moving perpendicular to the magnetic field is

$$\vec{E}_{\perp} + \vec{V}_{\perp} \times \vec{B} + \frac{m_i \nu_i}{e} (\vec{U}_{\perp} - \vec{V}_{\perp}) = 0 \qquad . \qquad (13)$$

The equation of motion for the electrons is unchanged

$$\vec{E}_{\perp} + \vec{V}_{e\perp} \times \vec{B} = 0, \qquad (14)$$

as are the equations of motion for the electrons and ions parallel to the magnetic field, Eqs. (2) and (3). The effect of the difference

12

between Eqs. (1) and (13) is that a neutral colliding with an ion can cause it to move perpendicular to the magnetic field as well as parallel to the field. This additional coupling of ion and neutral motions perpendicular to the magnetic field makes solving for the vector neutral wind possible. Therefore, the assumption that neutral motion is horizontal is no longer necessary in order to find the meridional component.

Equation (13) is easily solved for the neutral velocity

$$\vec{U}_\perp = \vec{V}_\perp - \frac{\Omega_i}{\nu_i}\left(\frac{\vec{E}_\perp}{B} + \frac{\vec{V}_\perp \times \vec{B}}{B}\right) \qquad (15)$$

or

$$U_x = V_x - \frac{\Omega_i}{\nu_i}\left(\frac{E_x}{B} + V_y\right) \qquad (16a)$$

$$U_y = V_y - \frac{\Omega_i}{\nu_i}\left(\frac{E_y}{B} - V_x\right) \qquad (16b)$$

where

$$\Omega_i = \frac{eB}{m_i}$$

and we are following a right-handed geomagnetic coordinate system such that $\hat{x}$ is horizontal to the magnetic east, $\hat{y}$ is at an elevation angle, $(90 - I)$, to the magnetic north, and $\hat{z}$ is up the magnetic field. The third component is given by Eq. (4b):

$$U_z = V_z + \frac{2kT_p}{m_i\nu_i}\sin I\left\{\frac{1}{T_p}\frac{\partial T_p}{\partial h} + \frac{1}{n_e}\frac{\partial n_e}{\partial h} + \frac{m_i g}{2kT_p}\right\} \qquad . \qquad (16c)$$

Below 150 km, we have assumed a mixture of 75-percent NO^+ ions and 25-percent O_2^+ ions, as mentioned earlier. This mixture is used in finding Ω_i, ν_i, and $m_i\nu_i$.

13

As in the F region, we may assume that the neutral velocity is entirely horizontal and use Eqs. (8) and (16c) to determine the component in the magnetic meridian

$$U_{MERID} = -\frac{U_z}{\cos I} \quad . \qquad (17)$$

This result is the same as Eq. (9). Or, we can combine U_y and U_z to find both the U_{MERID} and U_{VERT} components

$$U_{MERID} = U_y \sin I - U_z \cos I \qquad (18a)$$

$$U_{VERT} = U_y \cos I + U_z \sin I \quad . \qquad (18b)$$

U_{MERID} and U_{VERT} are two components of the wind in a modified geomagnetic coordinate system, modified in the sense that two components are horizontal. The third component is the wind in the magnetic zonal direction

$$U_{ZONAL} = U_x \quad . \qquad (18c)$$

While the three components of the neutral wind given by Eqs. (18a), (18b), and (18c) are useful, we are describing a neutral wind and, therefore, may also find it useful to transform to geographic coordinates

$$U_{EAST} = U_{ZONAL} \cos \delta + U_{MERID} \sin \delta \qquad (19a)$$

$$U_{NORTH} = U_{MERID} \cos \delta - U_{ZONAL} \sin \delta \qquad (19b)$$

$$U_{VERT} = U_{VERT} \qquad (19c)$$

where δ is the magnetic variation (~29° east at Chatanika).

So much for the formalism of finding $\vec{U}$ in various coordinate systems. An essential question now is how well can we find the initial three geomagnetic components. In U_x and U_y from Eqs. (16a) and (16b),

14

the components of the ion velocity V_x and V_y have been derived from sets of three line-of-sight velocity measurements. The electric-field components E_x and E_y are derived from ion-velocity measurements made above 150 km with the assumption that the magnetic field lines are equipotentials. Thus, from Eq. (1)

$$E_x = -V_y B \qquad (20a)$$

$$E_y = V_x B \qquad (20b)$$

where the ion components V_x and V_y are, as at lower altitudes, derived from sets of three line-of-sight velocity measurements. The remaining term, Ω_i/ν_i, or equivalently $eB/m_i\nu_i$, has for the moment to be calculated from models. The exact ion composition, whether NO^+ or O_2^+, has little effect on this term because of their similar masses and collision frequencies. To be consistent with ion composition elsewhere we have assumed 75-percent NO^+ and 25-percent O_2^+. They have been introduced by using an ion mass of 30.5 amu and a weighted collision frequency. The collision frequencies were calculated using the Jacchia [1971] model neutral atmosphere, which extends down to 90 km, and an exospheric temperature of 1000°K.

Below 110 km, ν_i is so much bigger than Ω_i that Eqs. (16a) and (16b) are greatly simplified such that the ion and neutral velocity components are equal.

In U_z from Eq. (16c), the ion component V_z can be measured directly or derived from sets of three line-of-sight velocity measurements. As in the F-region case, n_e and $\partial n_e/\partial h$ are determined from the measurements and the other terms from models. As also noted in the F-region discussion, the ion-neutral diffusion velocity below 225 km is very small. Indeed, for most of the E-region work, it is negligible.

B.   Fabry-Perot Interferometer Measurements

A Fabry-Perot interferometer can be used to measure the location in wavelength and the shape of a line emission profile. As with the radar spectrum, the location and, hence, Doppler shift of the line profile gives

15

the line-of-sight velocity and the shape gives the temperature. For the
F-region comparisons, observations were made of the 630-nm emission from
atomic oxygen. Because of the long lifetime of the excited state before
emission, collisions are sufficient so that the observations give both
the velocity and temperature of the neutrals, weighted by the volume
emission profile along the line of sight.

The 630-nm emission may arise from recombination [Wickwar et al.,
1974; Cogger et al., 1980] with the peak emission near 250 km or from
impact by energetic and secondary auroral electrons [Rees et al., 1969;
Roble and Rees, 1977] with the peak emission between 180 and 225 km.
That these measurements are integrated over a range of altitudes has
little or no impact because the altitude gradients in this region are
not very large, as shown by barium-cloud releases above 200 km [Meriwether
et al., 1973]. Thus the optical and radar measurements pertain to the
same altitude region.

The optical measurements were made by John W. Meriwether, Jr., using
the Michigan Auroral Observatory 15-cm Fabry-Perot interferometer. The
instrument as used in 1972 is described by Hays and Roble [1971]. The
pressure scanning system was modified to increase the instrument stability
for the 1973 observations. In this configuration, the interferometer is
described by Meriwether et al. [1975]. In addition, in 1973, a coaligned
photometer with the same field of view was used so that the Fabry-Perot
observations at each position in the wavelength scan could be normalized
to the potentially rapidly varying emission intensity.

The observations were made in the magnetic north, east, south, and
west as well as in the vertical. By assuming horizontal neutral motion,
the line-of-sight velocity measurements were converted to horizontal
velocities and the assumption of no vertical winds could be checked with
the vertical measurements. Critical to the Doppler shift or wind deter-
mination is the establishment of a zero-Doppler reference. This was done
with zenith observations near twilight on occasions when auroral activity
was small and then was extended through the observation period by measure-
ments by an argon emission at 629.81 nm from a laboratory source.

16

Another advance made possible by the change in pressure variation
was a change from sampling the whole free spectral range to one of
sampling at discrete positions on the profile. This selective sampling
increases the measurement efficiency and can adequately measure the velocity
and temperature. The method is illustrated in Figure 3 for two emission
profiles corresponding to different Doppler shifts. For the actual
measurements, seven positions were used.
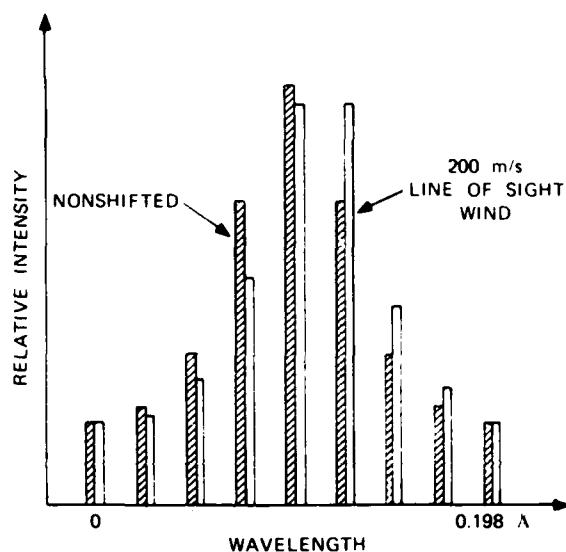
FIGURE 3   SCHEMATIC REPRESENTATION OF THE FABRY-
            PEROT SIGNAL FROM O(^{1}D) FOR NO DOPPLER
            SHIFT AND FOR 200 m/s LINE-OF-SIGHT
            VELOCITY

The processing of the data for velocity and temperature was based on
a least squares fit of a four-parameter function to the measurements.
This function was obtained from the convolution of the emission profile
with the instrument profile [Hays and Roble, 1971]. The instrument profile
itself was modeled from Fourier coefficients determined from measurement
of the 546.1-nm Hg profile excited by a high-frequency oscillator in a
discharge lamp cooled to 0°C.

Enough samples were taken at each wavelength so that the deduced
velocities had a precision of 20 m/s. The time resolution, therefore,
varied depending on the auroral intensity, but was usually the order of
5 to 10 min.

17

III   COMPARISON OF MERIDIONAL WIND MEASUREMENTS
BY THE RADAR AND FABRY-PEROT TECHNIQUES

In making any complicated measurement, comparison of the results
obtained by different methods is always advantageous.   Such comparisons
enable testing the assumptions that are not common to the different
methods.   During this study, we have been able to make the first compari-
son between meridional winds derived from the radar and the Fabry-Perot.
Neutral temperatures have previously been compared from these techniques
[Hays et al., 1970; Cogger et al., 1970], but the winds have not.

In the springs of 1972 and 1973, we obtained an extensive body of
correlative observations with the Chatanika radar and the MAO Fabry-
Perot.   The latter was set up at Ester Dome, almost magnetically south
of Chatanika 38 km away.   In Figure 4, we indicate the relative observ-
ing geometries for the two instruments in the magnetic meridian.   The
radar observations were along the magnetic field line and the Fabry-Perot
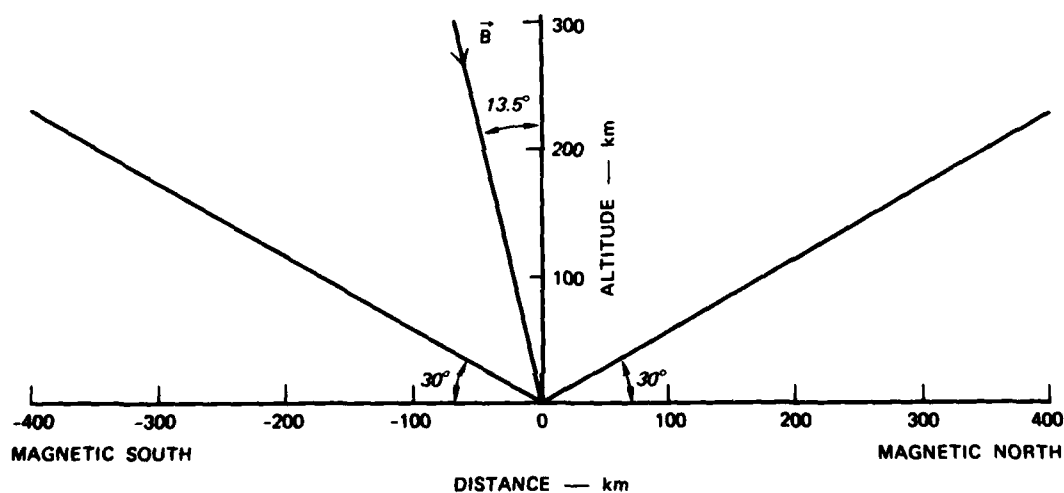
FIGURE 4   COMPARISON OF LOOK ANGLES FOR THE RADAR AND FOR THE FABRY-
PEROT. The radar line-of-sight was parallel to the magnetic field.   The Fabry-
Perot interferometer line-of-sight was at a 30° elevation angle to the magnetic
north or the magnetic south.

19

observations were at a 30° elevation angle to the north or to the south
and vertical. At 200-km altitude in the lower F region, the spatial
separation was about 400 km for the northward-looking Fabry-Perot measure-
ments and about 300 km for the southward-looking measurements.

In Figure 5, we show that, on average, we obtained very good agree-
ment between the meridional component of the wind measured by the radar
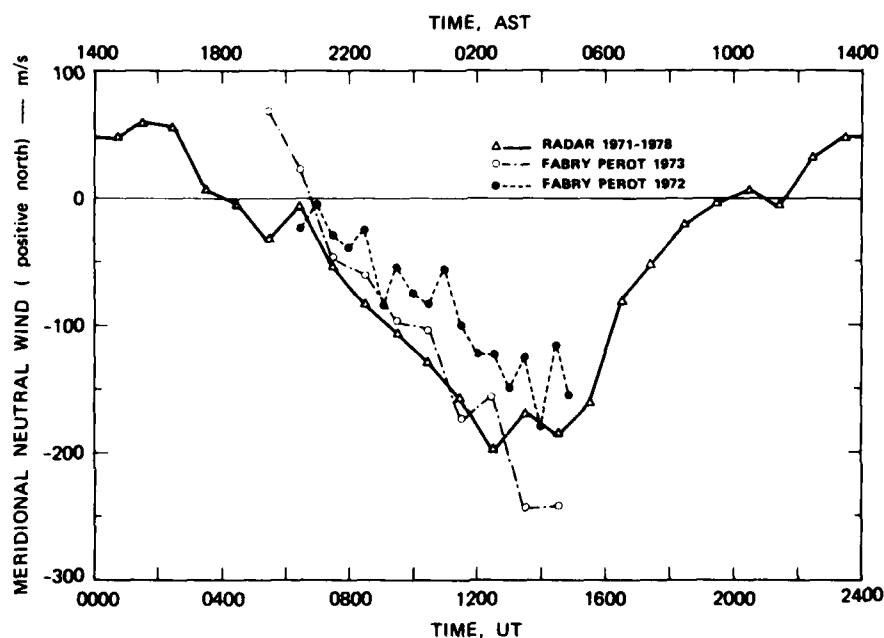
FIGURE 5   COMPARISON OF THE AVERAGE MERIDIONAL WINDS
            DETERMINED FROM THE RADAR DATA ACQUIRED
            BETWEEN 1971 AND 1978 AND FROM THE FABRY-
            PEROT 630-nm DATA ACQUIRED IN 1972 AND 1973

and the Fabry-Perot. The Fabry-Perot averages are for the springs of
1972 and 1973 (Table 1). The radar average uses most of the data ob-
served along the magnetic field lines between 1971 and 1978 (Table 2).
To decide whether this agreement is significant, we need to ascertain
that differences between the data sets are not significant. Thus, we
need to examine questions such as the effect of altitude, magnetic
activity, season, and solar cycle dependence.

20

Table 1

DATES OF FABRY-PEROT OBSERVATIONS ALONG WITH
GEOMAGNETIC AND SOLAR ACTIVITY PARAMETERS

Day	UT Date	ΣK_p	A_p	$S_{10.7}$
1	720122	30	25	123.2
2	720123	33	32	136.3
3	720125	25	17	131.8
4	720203	16	9	104.8
5	720214	23-	15	136.7
6	720215	21-	13	145.8
7	720217	26	22	168.2
8	720218	16	12	184.4
9	720219	19	14	190.6
10	720225	24	16	151.9
11	720228	11+	6	133.2
12	720302	18+	10	129.7
13	720303	24	16	131.1
14	720304	15	8	137.1
15	720306	19+	26	145.9
16	720307	37-	45	143.3
17	720309	19-	10	137.4
18	730223	40	48	91.4
19	730224	42-	54	93.6
20	730225	33	31	97.2
21	730226	35-	34	95.6
22	730227	37+	44	98.2
23	730301	26+	22	99.5
24	730303	22	14	97.8
25	730316	21-	12	106.9
26	730319	46-	82	96.7
27	730320	48-	80	91.0
28	730321	43-	58	87.4
29	730322	41	53	90.3
30	730323	40+	50	87.1
31	730324	40	49	89.4
32	730325	41-	50	40.0
33	730326	30+	32	88.6
34	730327	32	28	92.0
35	730328	29	22	94.2

Table 2

DATES AND TIMES OF RADAR OBSERVATIONS ALONG
WITH GEOMAGNETIC AND SOLAR ACTIVITY PARAMETERS

Day	Date (UT)	Times (UT)	ΣK	ΣK_p	A_p	\<AE\>	$S_{10.7}$
1	710909	1952 to 2400	14	14+	7	144	98.2
	710910	0000 to 1932	12	11	6	133	91.8
2	710923	0000 to 2300	3	4-	2	058	107.3
3	720120	1828 to 2400	18	17-	8	239	123.0
	720121	0000 to 0326	30	24-	22	350	127.9
4	720217	1908 to 2400	26	26	22	378	168.2
	720218	0000 to 0406	12	16	12	163	184.4
5	720307	0731 to 0850	32	37-	45	295	143.3
6	720406	1845 to 2400	13	14	8	119	118.1
	720407	0000 to 0900	16	16+	8	203	121.3
7	721013	0200 to 0800 / 1600 to 2400	27	28-	21	321	94.5
	721014	0000 to 0300	31	30+	26	336	97.0
8	721116	0200 to 2400	37	33+	31	417	89.6
9	721215	0100 to 2400	26	28-	29	295	116.1
10	730223	0821 to 1159	41	40	48	546	91.4
11	730226	0543 to 1240	40	35-	34	424	95.6
12	730301	0830 to 1540	30	26+	22	333	99.5
13	730303	0700 to 1300	21	22	14	172	97.8
14	730321	1121 to 1520	45	43-	58	705	87.4
15	730322	0700 to 1500	43	41	53	623	90.3
16	730326	0700 to 1100	32	30+	32	378	88.6
17	730327	0900 to 1400	34	32	28	463	92.0
18	730328	0800 to 1200	30	29	22	383	94.2
19	730401	0525 to 1749	44	43-	91	590	115.0
20	730530	0700 to 1200 / 1700 to 2300	0	4+	3	051	90.8
	730531	0000 to 0600	07	9-	4	081	87.2
21	740116	0000 to 2400	28	24-	15	268	90.0
22	750917	0000 to 0600 / 1500 to 2400	17	20+	13	--	74.8
23	751015	0900 to 2400	10	9+	5	--	80.3
	751016	0000 to 0100	15	18	10	--	78.5
24	760118	1000 to 1600	20	17-	9	144	76.7
25	760120	1100 to 1600	19	19-	11	136	74.6
26	760831	2200 to 2400	15	11	5	--	73.8
	760901	0000 to 0500	17	19-	10	--	76.3
27	780313	0700 to 1600	25	21+	12	--	160.9
28	780314	0900 to 1500	19	19	10	--	160.5
29	780316	0700 to 1700	31	29+	24	--	143.3
30	780317	0800 to 1600	34	30+	25	--	135.4
31	780318	0900 to 1500	31	29+	24	--	132.3
32	780319	0900 to 1600	27	23	15	--	128.1
33	780320	0400 to 1500	19	17+	9	--	125.3
34	780413	0400 to 2200	25	27+	24	--	145.6
35	780414	0000 to 1900	37	40	51	--	139.1

22

In Figure 6, we show mean radar measurements based on one-hour averages centered around three altitudes--170, 225, and 280 km--and the distribution of measurements at these altitudes. The mean curve is determined from these three curves weighted by the number of observations. During the nighttime, when these comparisons could be made, more measurements were taken at the lower two altitudes, which were in keeping with the expected altitude of the Fabry-Perot measurements for auroral excitation. Hence, there is good agreement in altitude between the two data sets.

In Figure 7, we show the distribution of measurements as a function of magnetic activity, K_p. The situation was more active for the 1973 Fabry-Perot measurements than for the 1972 Fabry-Perot measurements, and, perhaps, a little more active than for the radar measurements. However, the differences in the distributions of data as a function of magnetic activity are small. In addition, as we see in a later figure, almost all the data were obtained within a month of the equinox. We have also divided the data set into two parts and compared the averages to look for indications of solar-cycle effects. No effects large enough to be detected were found.

Thus, from the point of view of altitude, magnetic activity, season, and solar cycle, we have good agreement for the observing conditions. Therefore, the good agreement among the averaged meridional winds in Figure 5 is highly significant.

In addition to the comparison of averaged winds, we have a few cases of simultaneous or interleaved observations. They are shown in Figure 8. Each panel has two sets of curves: the upper is for the Fabry-Perot, the lower is for the radar. The smooth curves, which are an average of the radar and Fabry-Perot curves in Figure 5, serve as a reference for the two data sets. With a few notable exceptions, the agreement is good.

These exceptions are very important. In particular, we have been able to examine the data from 1 March 1973 between 1000 and 1100 UT and between 0400 and 0500 UT because the Fabry-Perot measured the vertical as well as meridional winds on that day. We found out that in the auroral
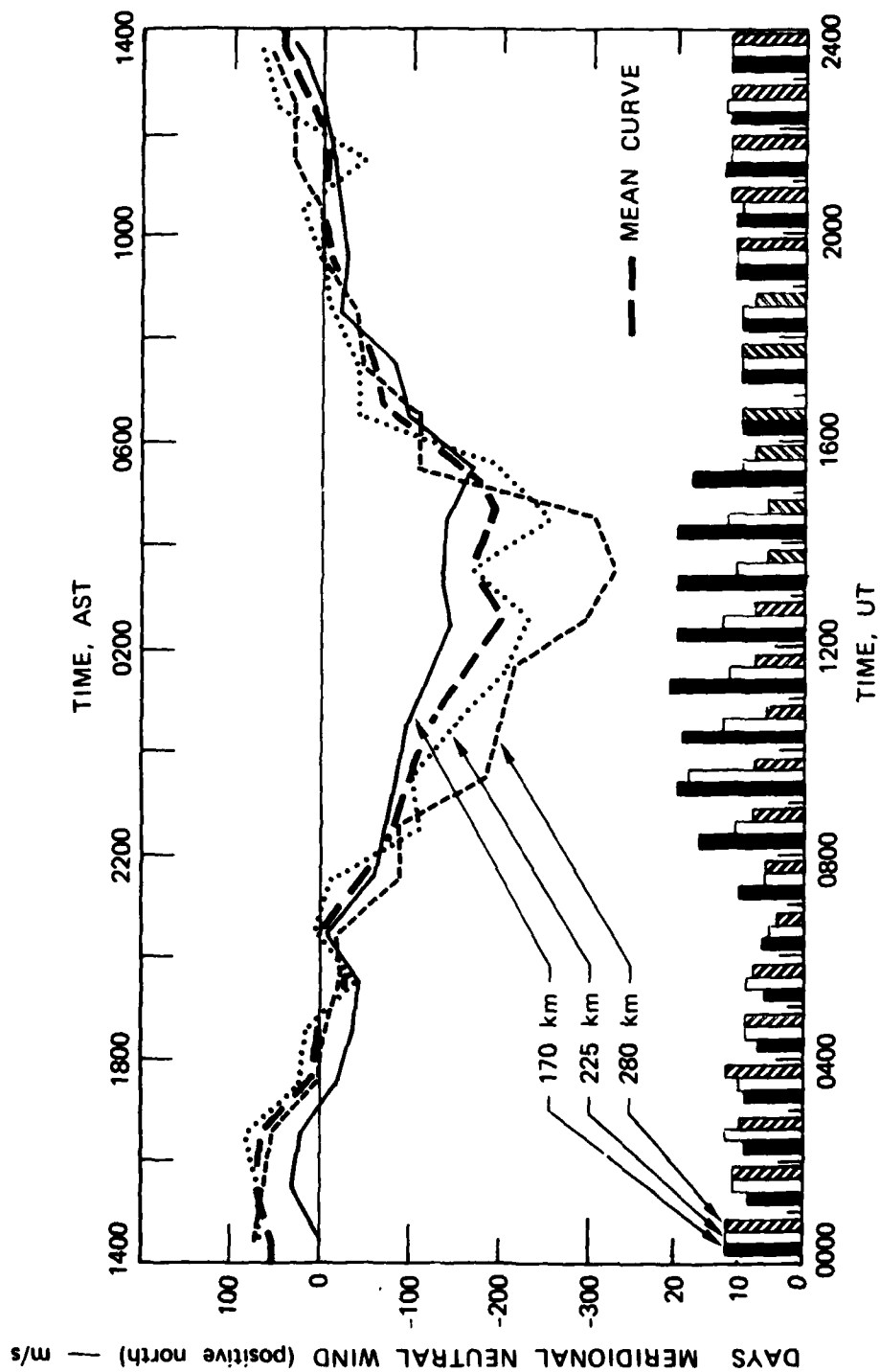
FIGURE 6   COMPARISON OF THE MERIDIONAL WIND DETERMINATIONS FOR 170, 225 AND 280 km AND THE OVERALL MEAN WIND. Also included is a histogram of the number of days on which the data existed for the three altitudes.

24

FIGURE 7   COMPARISON OF MAGNETIC ACTIVITY
            K_p FOR THE RADAR AND FABRY-PEROT
            INTERFEROMETER DATA IN FIGURE 5

25

FIGURE 8   COMPARISON OF SIMULTANEOUS DETERMINATIONS OF
THE MERIDIONAL WIND WITH THE RADAR AND FABRY-
PEROT. For reference purposes a smooth average curve from
the curves in Figure 5 is included with each set of measure-
ments.

26

region we cannot always assume that the wind is horizontal. Moreover, the radar is much more sensitive to the vertical component of the wind t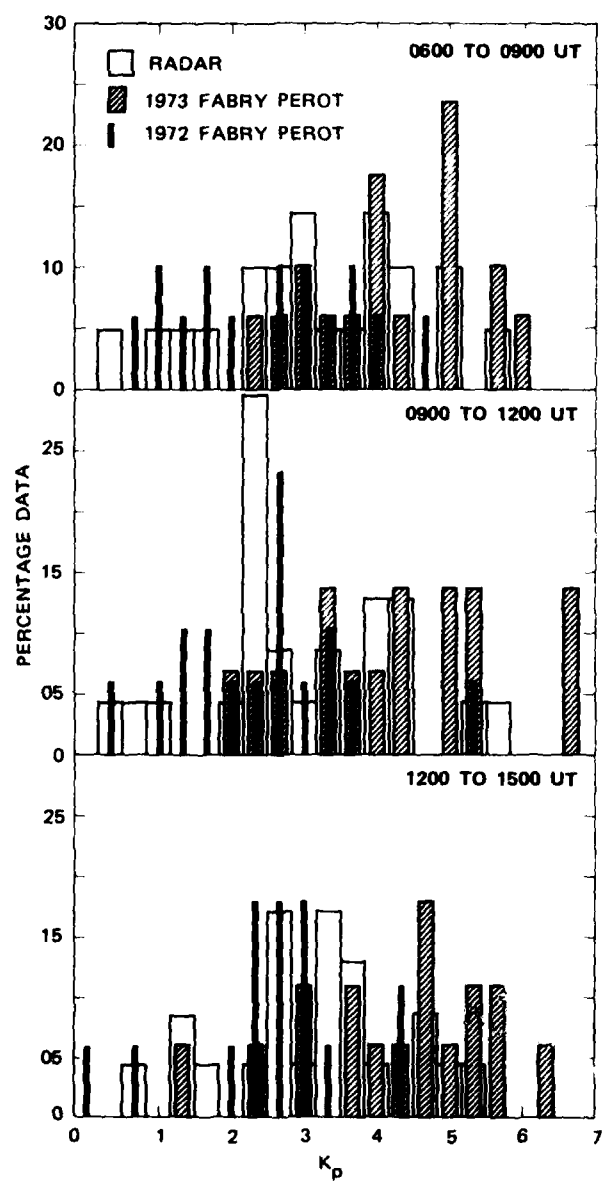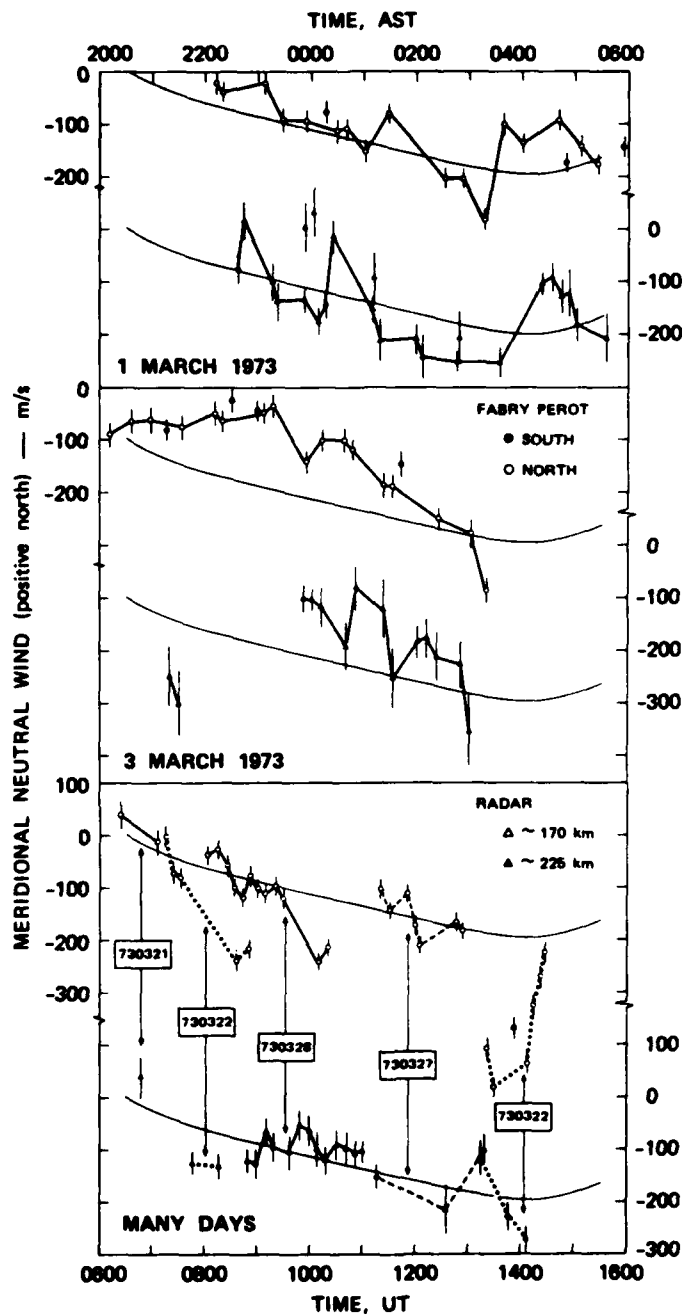han the Fabry-Perot when at a 30° elevation angle. We discuss these vertical winds or gravity waves in Section V. These winds have a characteristic time and altitude behavior that we have identified, enabling us to remove them from the average data. Indeed, before we removed these effects from the average data, we did not have the good average agreement shown in Figure 5.

Thus the radar/Fabry-Perot comparisons have proved very useful. They have enabled us to find occasions when the assumption of a horizontal wind is not valid. More generally, though, they show good agreement between the two methods. This agreement strengthens our confidence in both techniques and in particular enables us to make comparisons between the techniques. For instance, we can look for latitudinal gradients in the meridional winds where the Fabry-Perot measures to the north or south, and the radar, along the field line. Or, as we do in Section VI, we use the Fabry-Perot to measure the zonal neutral wind and the radar to measure the ion drift.

IV F-REGION MERIDIONAL WIND

As already shown in Figure 5, we have obtained a mean meridional
wind for the F region above Chatanika. This mean wind gives a reference
for examining subsets of the total data set and specific days. As indi-
cated in the introduction, one of our first interests is whether the
meridional wind varies with magnetic activity. To examine this point,
we divided the data set into the data with K_p values less than 3+ and
greater than 4-. The results are presented in Figure 9. In the bottom
panel we show the results for high activity at the three altitudes for
$K_p \geq -4$; in the next-to-bottom panel, we show the results for low activity
at the three altitudes for $K_p \leq 3+$. There are differences between these
curves: to make the differences more obvious, we have averaged together
the three altitudes and presented the results in the second panel. In
the afternoon and evening, between 1200 and 2300 AST[*] (2300 and 0900 UT),
the difference is not significant. But during the night and morning from
2300 to 1200 AST, the difference is significant. The largest increase occurs
to the south during the night between 0000 and 0600 AST and is on the order
of 100 m/s. To further examine these differences, we have only looked at
the lowest altitude in the top panel, which shows the average meridional
wind for $K_p \leq 3+$ and $K_p \geq 4-$ for 170 km, with the same results. Thus, under
all conditions we have a net velocity to the south and we have an increase
in that velocity during periods of magnetic activity.

The next question is whether there is a discernable seasonal varia-
tion. In our data sample along the magnetic field line, we do not have
enough cases of winter and summer measurements to establish a seasonal
pattern. However, we can divide the data by season and see if the data
that we do have are consistent with the theoretical productions. In

---

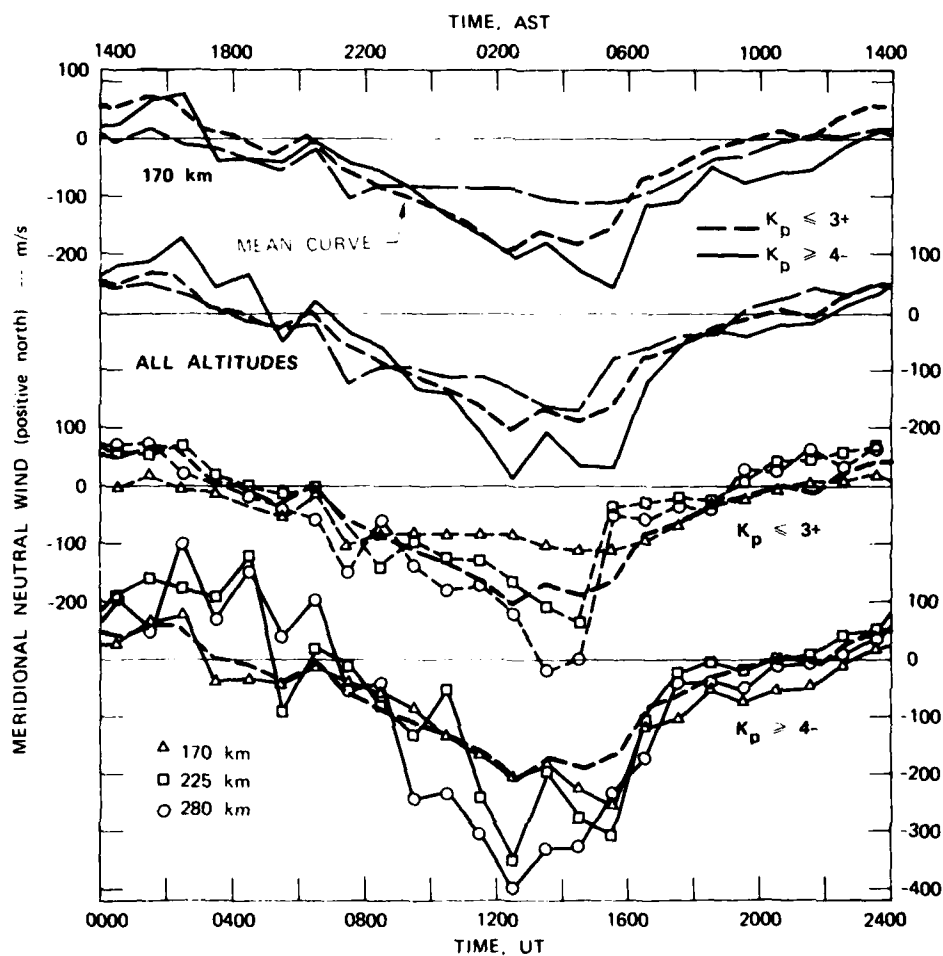[*]Alaska Standard Time

29

FIGURE 9   VARIATION OF THE MERIDIONAL WIND WITH MAGNETIC ACTIVITY.   For reference, each panel has the average meridional wind.

Figure 10 we show the results. As indicated in the previous section, most of the data are from the equinoxes. There is only one summer day, but on that day the wind is approximately 100 m/s stronger to the south than on the other days. This effect is not likely to be caused by magnetic activity because this is the quietest day in the whole data set. Thus, this shift is consistent with the seasonal predictions that arise from a summer-winter pressure gradient caused by greater upper atmospheric temperatures in the summer hemisphere than in the winter hemisphere [Dickinson et al., 1981].

Slightly more data are available from the winter period. During the day, the data are very similar to the mean data, but during the night, the southward velocities are reduced approximately 100 m/s. Again, this is the same direction as predicted by theory.

The observed results can also be compared to theoretical calculations. We first compare the observed results with the calculations by Straus [1978] shown in Figure 11. The upper set of curves includes the theoretical curves for no magnetic activity and the usual mean curve from the observations. The "geomagnetic" theoretical curve combines the geomagnetic meridian. The lower set of curves includes the "geographic" curve from above along with another "geographic" curve for high magnetic activity. Converting this last curve to a "geomagnetic" one is difficult, as described below. Also included are the curves for low and high magnetic activity obtained from the observations.

One difficulty in making these comparisons is that the theory uses a geographic coordinate system and assumes that the geomagnetic and geographic axes coincide. In reality, they do not coincide. Indeed, at Chatanika, the variation in the magnetic field is 29°. However, for quiet conditions, there should be little magnetic control, thereby enabling us to formally rotate coordinate systems. Accordingly, we have presented Straus' calculations in both geomagnetic and geographic coordinates in the top set of curves. We find reasonable agreement at night between theory and experiment for the magnitude of the southward wind. The agreement is also good for the phase of the wind, particularly for geomagnetic coordinates.
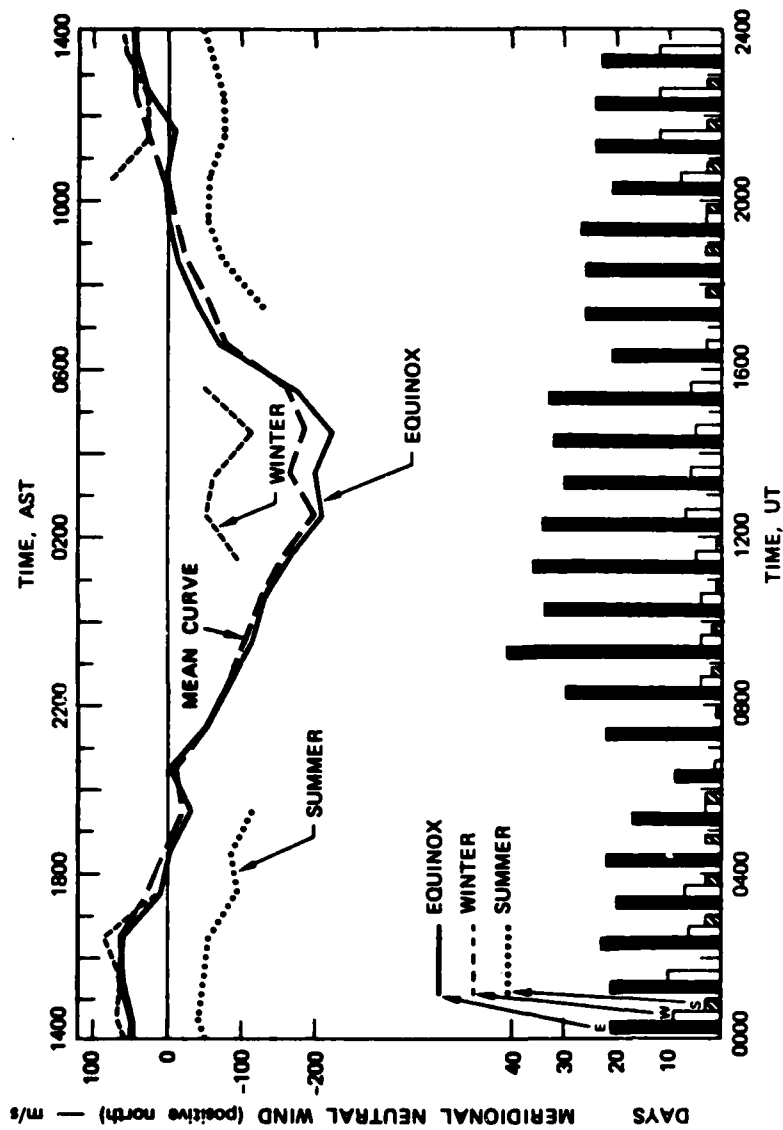
31

FIGURE 10   VARIATION IN AVERAGE MERIDIONAL WIND AND THE DISTRIBUTION OF DATA POINTS AS A FUNCTION OF SEASON
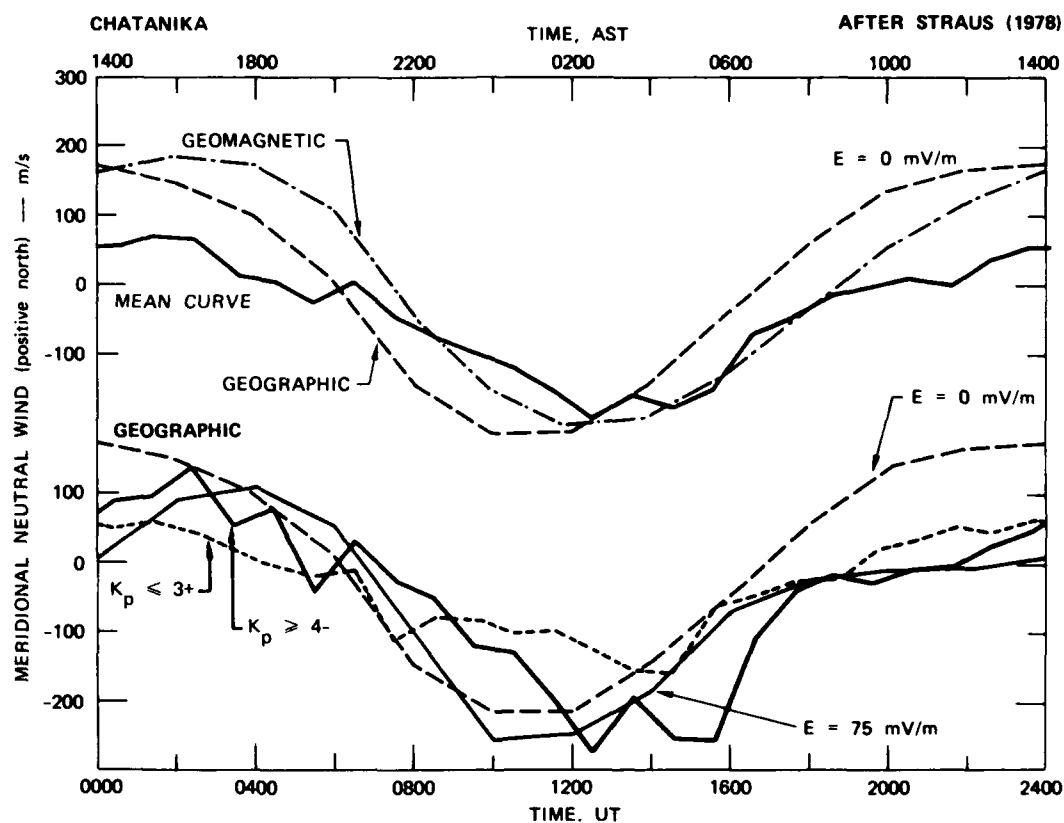
32

FIGURE 11   COMPARISON OF MERIDIONAL WIND OBSERVATION WITH THEORETICAL
CALCULATIONS, [Straus, (1978)]

33

However, the northward wind during the day is very different; the observations are considerably smaller. We wonder if an additional daytime heat source exists poleward of Chatanika that leads to greater daytime pressures. On the basis of satellite drag data, Olson and Moe [1974] have suggested that the cusp is such a heat source.

In the model, variations in magnetic activity are included by varying the polar cap electric potential. The effects of this change are shown in the bottom part of Figure 11. Because effects are present that naturally occur in the two coordinate systems, we are unable to rotate to the geomagnetic coordinates. We see a considerably reduced daytime wind that is much more in keeping with all our observations. Thus, a high-latitude heat source on the dayside always appears to be present. The model shows only a small variation between the active and quiet conditions at night, contrary to our observations. But as for quiet conditions the agreement is, in large part, relatively good.

We next compare the observations with calculations by Hays et al. [1979], Figure 12. The upper set of curves includes the theoretical curves obtained by using the MSIS model atmosphere. The "geographic" curve has been modified as in Figure 11. Also included is the usual mean curve from the observations. The lower set of curves includes the latter two curves plus one for the theoretical meridional wind when ion drag is added. It also includes a curve that was obtained when the neutral atmosphere temperatures were modified to enable the theoretical wind to match the observations.

In their paper, Hays et al. [1979] attempted to match calculations to observations. For observations, they used the average 1972 neutral winds from the Fabry-Perot and the average ion velocities from the radar. In the first step of the comparison, they used the winds calculated with the MSIS model of the neutral atmosphere. Again, we rotated the results from geographic to geomagnetic coordinates, Figure 12. We find reasonable agreement in phase and nighttime magnitude. The biggest difference occurs in the morning hours where, once again, the observed winds are more southward than the model calculations. In the second step, the authors
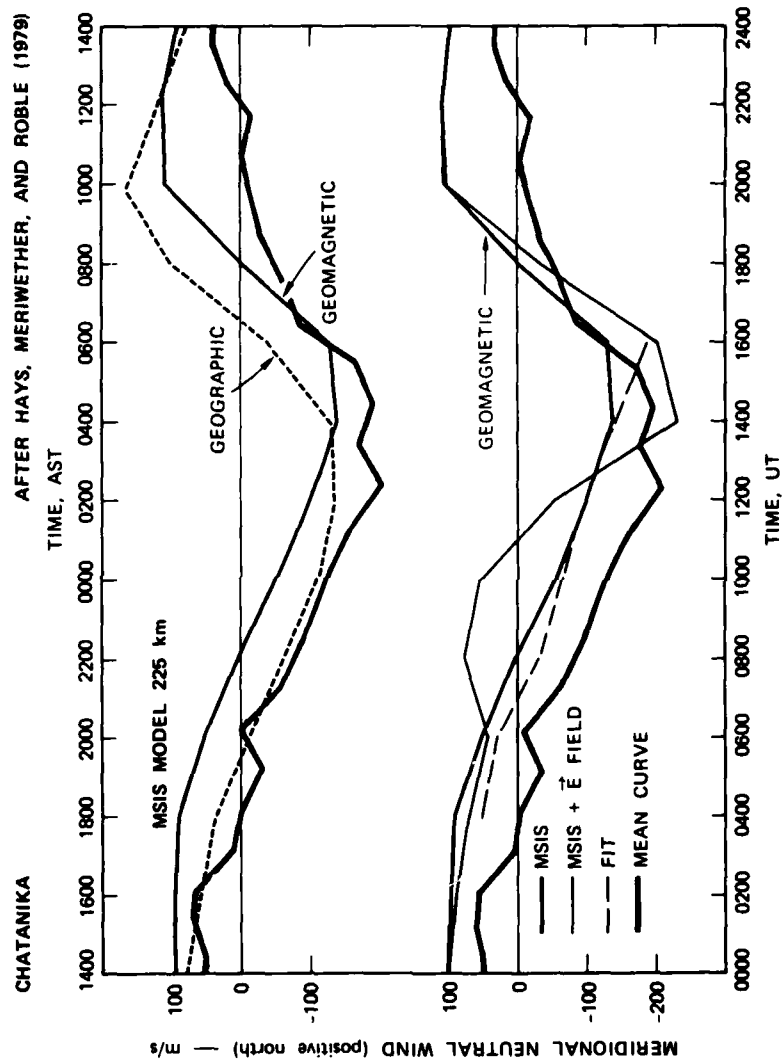
34

FIGURE 12   COMPARISON OF MERIDIONAL WIND OBSERVATIONS WITH THEORETICAL CALCULATIONS
FROM HAYS et al. [1979]

35

included the mean ion-velocity variation and obtained a much greater difference between calculated and observed winds. In the third step, they postulated that the remaining differences had to be caused by heat sources in the auroral region. They included nighttime heat sources in such a way that the calculated winds, including the effects of ion convection, were forced to agree with the winds obtained from the Fabry-Perot measurements.

In Figure 13(a) we show the required exospheric temperature distribution. Instead of following the MSIS temperature curve, Figure 13(b), that decreases gradually during the night, they required a temperature distribution that increases during the night. While this behavior is contrary to all the models, it is similar to the behavior of the temperature seen on occasion at Chatanika. In Figure 14, we show the exospheric temperature variation obtained for two sets of days at Chatanika from the radar data. In the upper set, the variation follows that of the Jacchia 1971 model (which behaves similarly to the MSIS model); whereas in the other set, the temperature is substantially greater in the early morning than in the late evening and in the model. Thus, it appears that considerable heating can occur poleward of Chatanika during the night. This behavior is similar to that in Figure 13(a). Indeed, if this heating helps drive the meridional wind, it must occur on the poleward side of the auroral oval or in the polar cap. If it occurred in the middle of the oval or on the equatorward side, then, under conditions of great magnetic activity, it would be south of Chatanika where it would act to reduce the meridional wind velocity. That effect would be contrary to our observations.

Thus, from this comparison of observation with theory, it appears that there is the need for both a daytime and a nighttime heat source that would be situated poleward of the auroral region.

Before leaving the meridional wind, a look at the data from several individual experiments may be instructive. In Figure 15, we show the wind from a magnetically very quiet day.

36
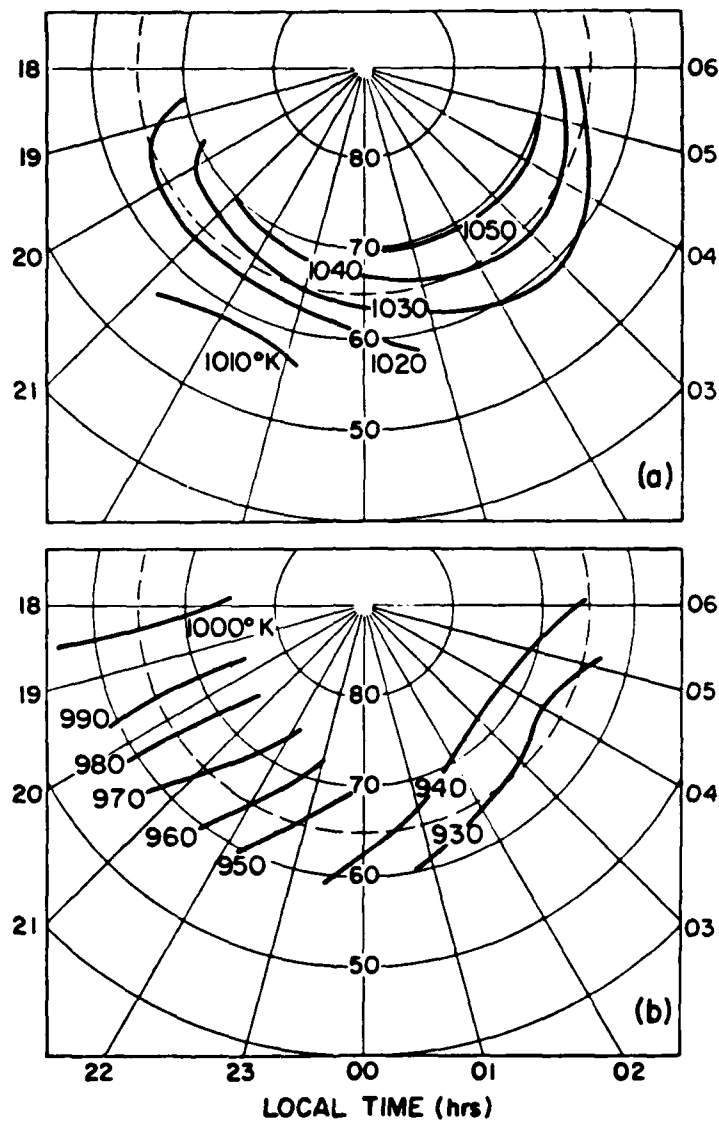
AFTER HAYS, ROBLE, AND MERIWETHER (1979)

FIGURE 13   EXOSPHERIC TEMPERATURES [Hays et al. (1979)]. Part (b) shows the
temperatures from the MSIS model that were used to obtain the first
theoretical calculation in Figure 12. Part (a) shows the temperatures that
had to be adapted to obtain agreement with the Fabry-Perot observations
in Figure 12.
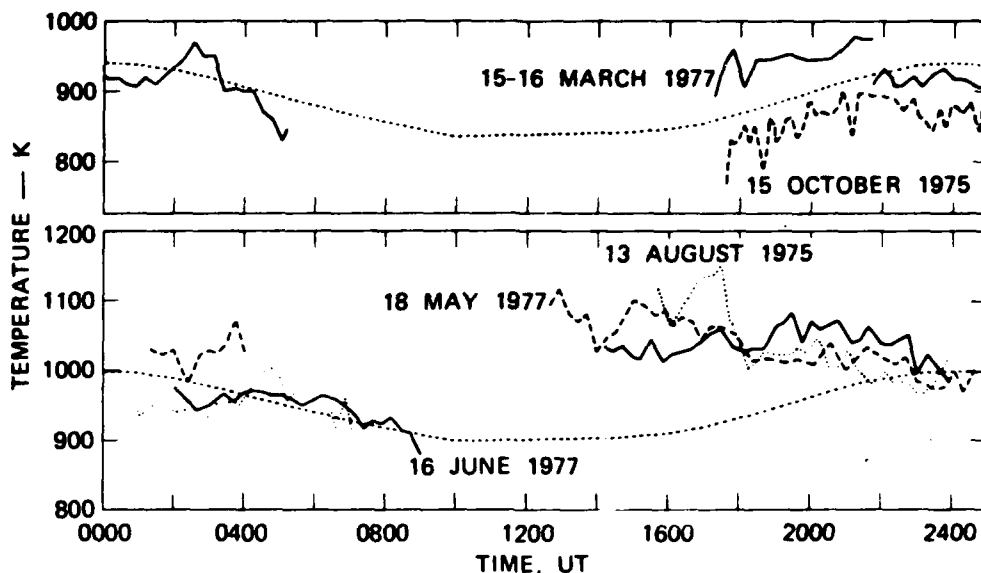
37

T∞ FROM CHATANIKA AND JACCHIA (1971)

FIGURE 14   EXOSPHERIC TEMPERATURES FROM CHATANIKA

In Figure 16, we show the wind from a 36-hour period. During the first 12 hours, the geomagnetic activity is low; during the last 24 hours, it is high. In Figure 17, we show the wind for a very active 12-hour period. In all three figures, the mean curve from Figure 5 is included for comparison. The data points were determined at 10-min intervals and were omitted if uncertainty was greater than 50 m/s. The possibility of contamination from vertical winds associated with gravity waves is discussed in Section V. However, we note here that the large spikes in the data, such as at 1530 UT on 14 April 1978 and at 1510 and 1640 UT on 1 April 1973, are examples of these gravity waves.

On the first day, Figure 15, the data are close to the mean curve, but tend to show winds that are not as strong to the south. On the last day, Figure 17, the nighttime winds, even at the lowest altitude, are considerably stronger to the south than the mean. Between 1700 and 1900 UT in the morning on 14 April 1978, the winds are considerably stronger to the south than on the preceding day, as we might expect because of the greater magnetic activity. However, between 0400 and 0800 UT in the early evening on 14 April, the winds are stronger to the

38

FIGURE 15   MERIDONAL WINDS AT CHATANIKA FOR 9 AND 10 SEPTEMBER 1971

39
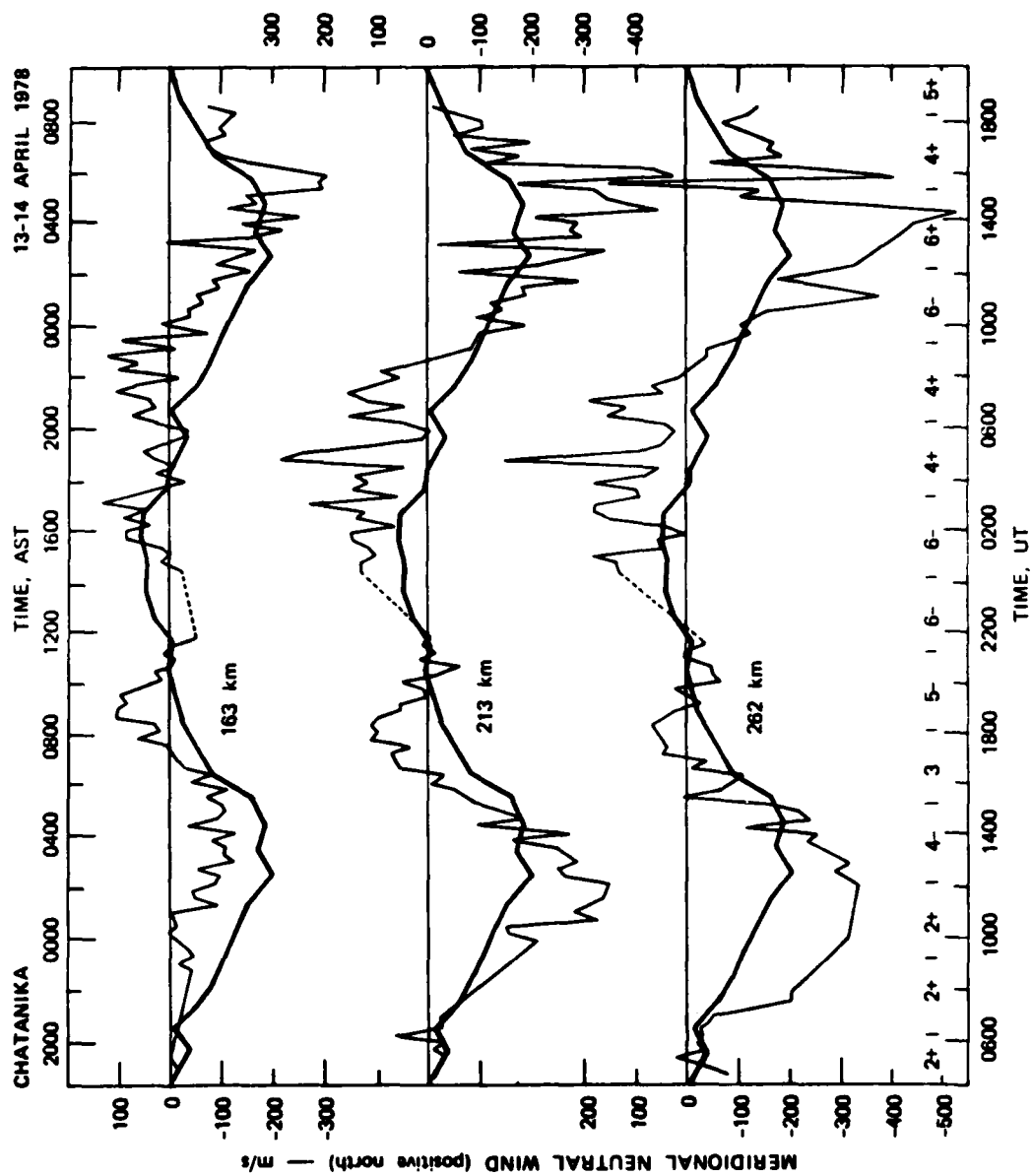
FIGURE 16   MERIDIONAL WINDS AT CHATANIKA FOR 13 AND 14 APRIL 1978

40
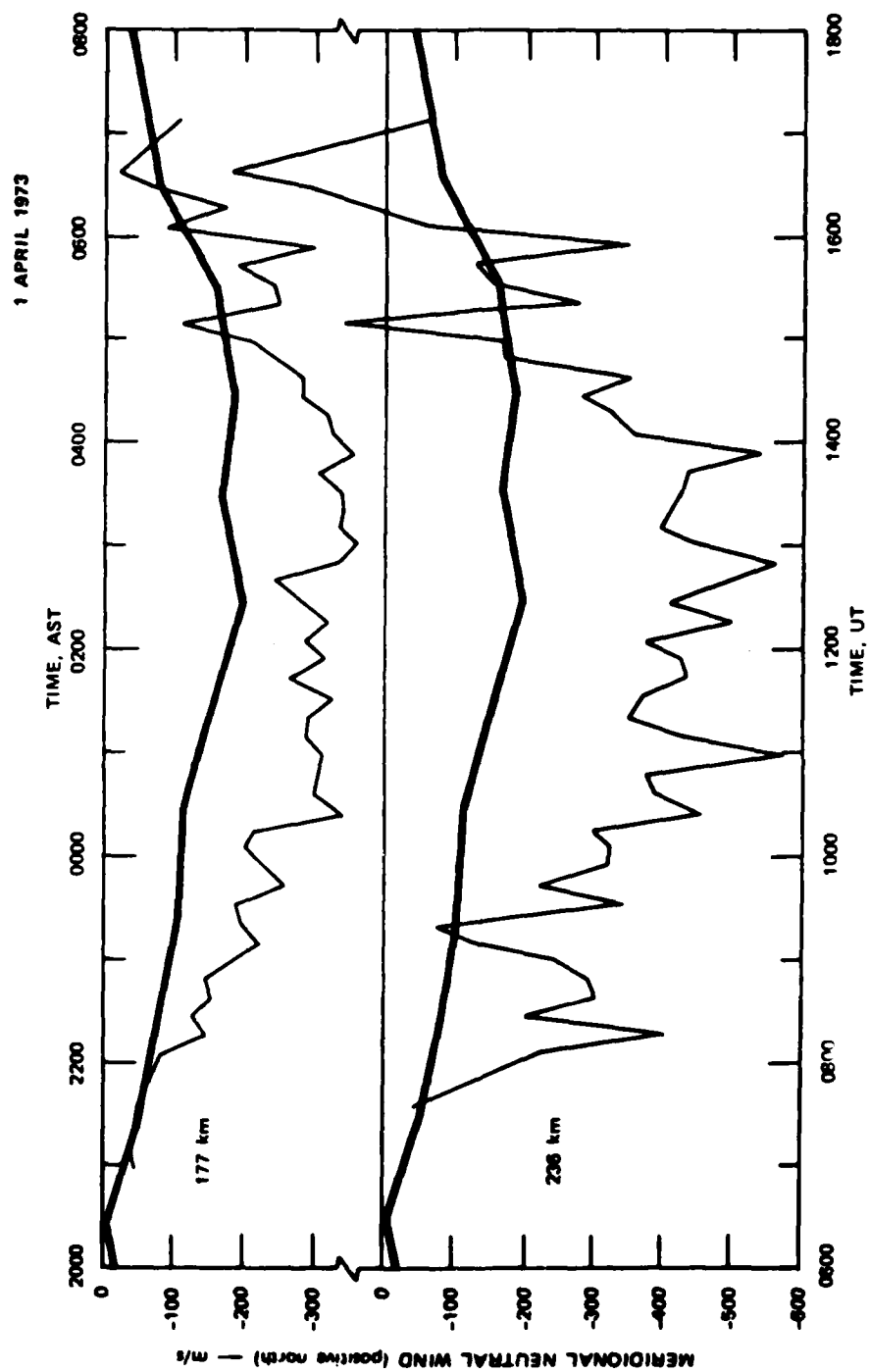
FIGURE 17   MERIDIONAL WINDS AT CHATANIKA FOR 1 APRIL 1973

41

north than on the preceding day despite the greater magnetic activity. Thus, we see considerable day-to-day variability in addition to the effects of magnetic activity.

An altitude gradient seems to be present in these meridional winds, particularly at night, just as in the averaged data in Figure 6. During the night, the southward wind increases significantly with altitude. A small phase shift may be present with the lowest altitude responding slightly later. During the day, from roughly 1800 to 0600 UT, the wind at the upper two altitudes often appears stronger to the north than at the lowest altitude.

V F-REGION VERTICAL VELOCITIES AND GRAVITY WAVES

As discussed in Section II, one of the requirements in making Fabry-Perot observations is to establish a zero reference. Because vertical motion of the neutrals exceeding 1 m/s were unexpected [Hays et al., 1973], vertical measurements were made to establish that reference. However, these results showed more variation in this reference than expected. Therefore, measurements were also made of the argon emission profile from a laboratory source. The bottom curve in Figure 18 shows the apparent drift of the Fabry-Perot velocity determinations for a five-hour period from such measurements. That drift is long term with small noise fluctuations of the expected magnitude. Because this smoothly varying long-term drift is determined each night and removed during the data analysis, the variations in the zero reference seem to be caused by vertical velocity disturbances.

A clear example of such a vertical velocity disturbance appears in the data for 19 March 1973 presented in Figure 18. A large downward velocity appears centered at 0900 UT. This is a good example because the time resolution is good before, during, and after the disturbance and because the disturbance is large compared with the measurement uncertainty. By contrast, on 30 March 1973, the indication of such an event is not clear. (Without more data, we cannot say what is happening at the end points.) Usually, vertical measurements were not made as frequently as on these two days. A more typical day is 1 March 1973, which is also shown in Figure 18. A large disturbance appears at 1000 UT and perhaps a smaller one at 1430 UT. However, in both cases, the event is marked by only one data point, unlike 19 March 1973.

Thus, from the Fabry-Perot data, large disturbances appear in the vertical velocity of the order of 50 to 100 m/s that have a duration of about an hour. They do not appear attributable to instrumental drift. Not only is the instrumental drift accounted for by the measurement of a
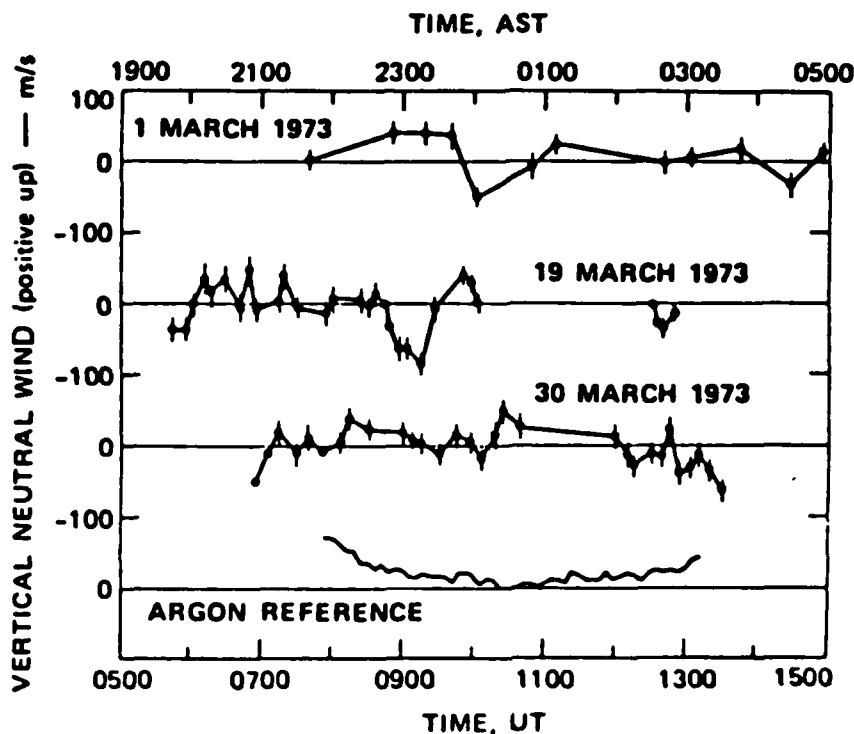
43

FIGURE 18   VERTICAL NEUTRAL WIND MEASURED WITH THE FABRY-PEROT
INTERFEROMETER

stable laboratory source, but it varies with a time scale much longer
than the hour characteristic of these disturbances. Because of the paucity
of measurements and the unexpected nature of the result, we have looked
for confirmation of the finding from a totally independent measurement.

That confirmation has come from the Chatanika radar measurements.
As discussed in Section II, radar measurements parallel to the magnetic
field are sensitive to neutral velocities. Usually, these velocities are
assumed horizontal, yet because of the 76.5° dip angle, the radar is four
times more sensitive to vertical velocities, i.e., the projection of a
given vertical velocity onto the magnetic field is four times as big as
the projection of a horizontal velocity of equal magnitude. The implica-
tion, then, is that, if the radar data were reduced as though it were
horizontal, a 50-m/s vertical disturbance would appear as a 200-m/s dis-
turbance in the meridional wind. Such a large disturbance with a one-hour

44

duration is unexpectedly large for the horizontal neutral wind and would clearly show up.

By contrast, the Fabry-Perot measurements at a 30° elevation angle are much less sensitive to a vertical velocity. Returning to the example used above, a 50-m/s vertical disturbance will appear as a 20-m/s disturbance in the meridional wind. Such a small variation will not stand out compared with the variations in the meridional wind. However, it might be detectable by two Fabry-Perot interferometers measuring north and south or east and west.

In Figure 19 we again show the correlative meridional winds obtained with the two instruments. As noted in Section III, the agreement in general is good, but there are notable exceptions. We concentrate on 1 March 1973 because of the existence of Fabry-Perot measurements at both 30° and 90° elevation angles. The largest discrepancy occurs between 1000 and 1100 UT. In particular, a 150-m/s change appears in the radar velocity between two successive data points about 10 min apart while no such change appears for the Fabry-Perot velocities. To examine this situation, we have replotted the vertical Fabry-Perot data in Figure 20 and transformed the radar data to vertical after subtracting the mean meridional wind used in Figure 19. This manner of accounting for the meridional wind is somewhat arbitrary and implies that we believe the neutral velocities change slowly. Alternatively, we can subtract interpolated Fabry-Perot observations from the radar results and convert to vertical.

In Figure 20, between 1000 and 1100 UT, large downward velocity disturbances were measured with both instruments. They occur at approximately the same time and have magnitudes that are somewhat similar. From what we will see later, the smaller velocity variation for the radar implies a lower altitude. Again between 1400 and 1500 UT, a downward velocity disturbance appears in the Fabry-Perot data. During the same period, correlated change appears in the radar data, but at least part of that change is probably related to a decrease in the southward meridional wind measured by the Fabry-Perot.
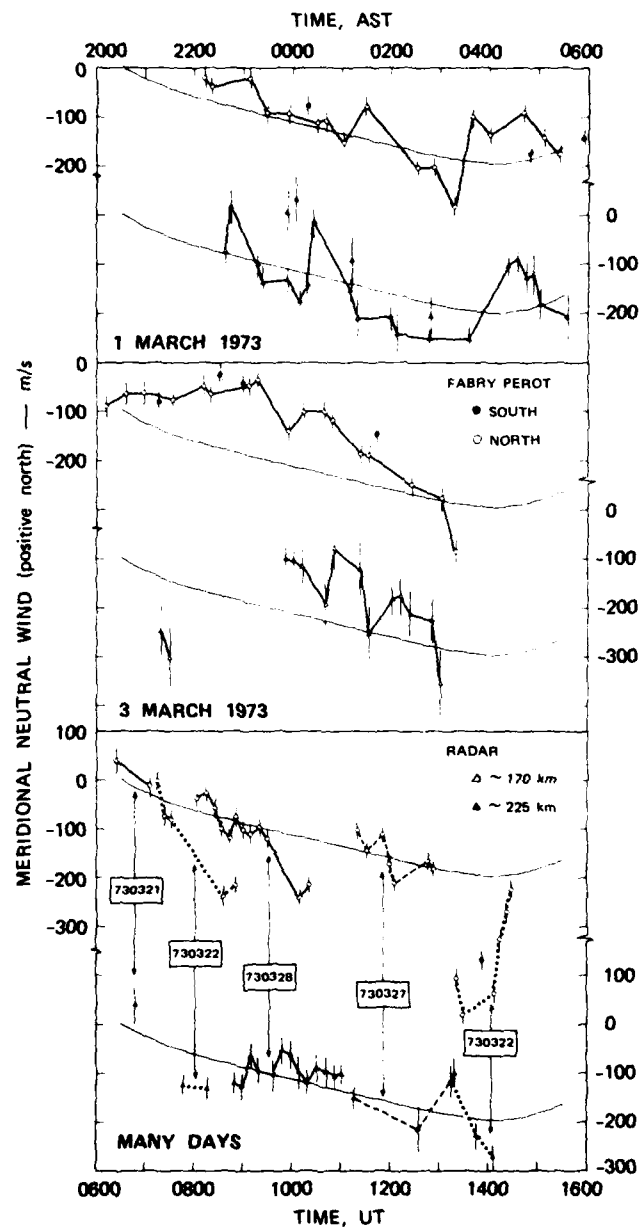
FIGURE 19   COMPARISON OF SIMULTANEOUS DETERMINATIONS OF
MERIDIONAL WIND MADE WITH THE RADAR AND FABRY-
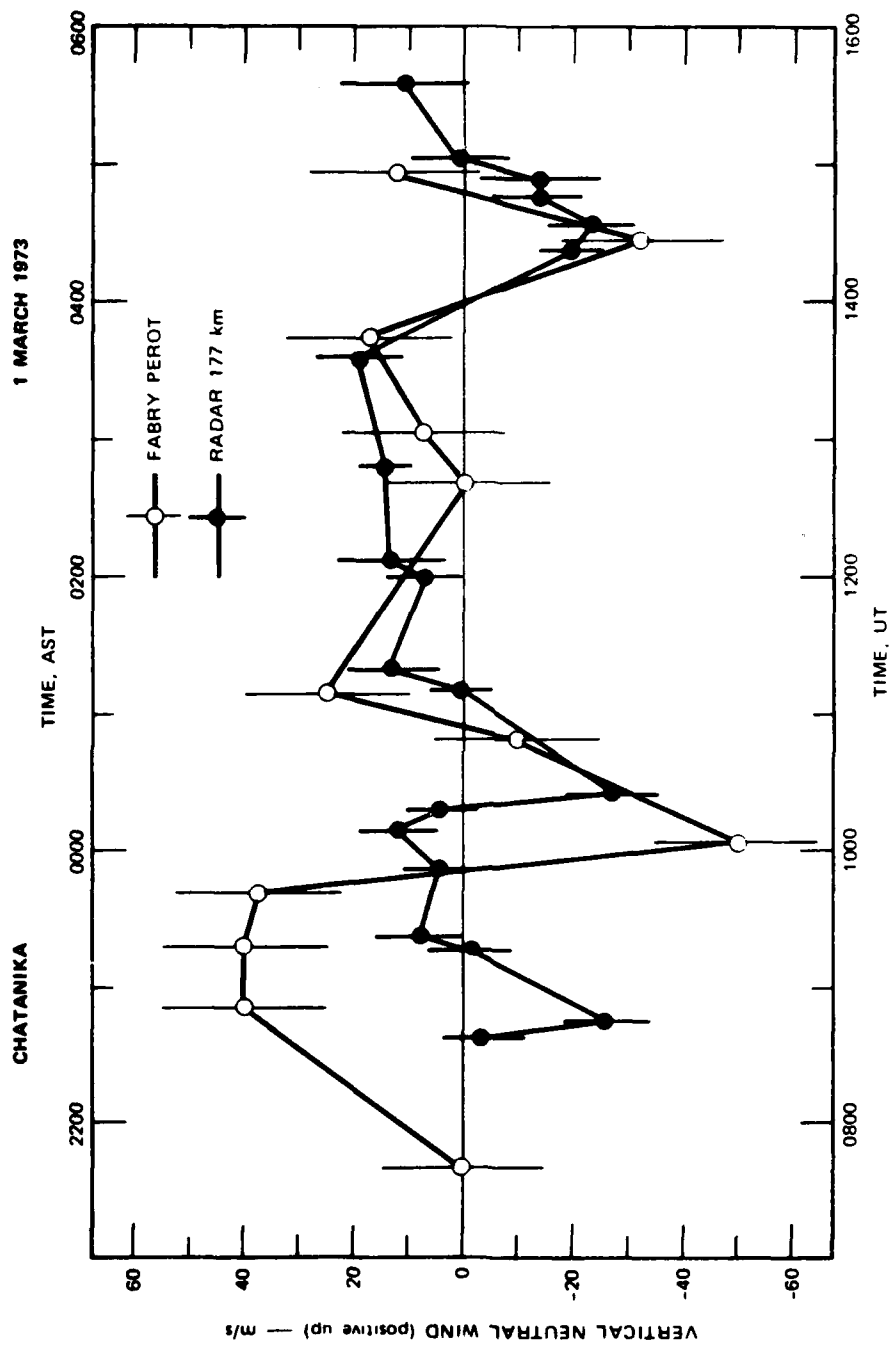PEROT INTERFEROMETER

46

FIGURE 20   COMPARISON OF SIMULTANEOUS DETERMINATIONS OF THE VERTICAL WIND MADE WITH THE
RADAR AND FABRY-PEROT INTERFEROMETER ON 1 MARCH 1973

47

Thus, in this limited correlative data set, a variation appears
in the radar velocities at the time of vertical Fabry-Perot motions.
This agreement in time and direction is important support for the Fabry-
Perot measurements of large vertical disturbances. In addition to this
direct evidence, much more indirect evidence exists. As previously
pointed out, a vertical disturbance will have a much greater effect on
the meridional wind deduced from the radar than from the Fabry-Perot.

Indeed in Section IV, the Fabry-Perot data show no signs of large
disturbances. The radar data also show no signs of disturbances, but
that is because they have been eliminated. However, on many occasions
large fluctuations are indeed in the radar data when we analyze them for
meridional winds. In Figure 21 we show a case from 26 February 1973. At
177 km, two cases are centered about 0920 and 1210 UT, when a large per-
turbation appears in the meridional wind with a duration approaching one
hour. These data are much better than the data from 1 March 1973 in that
the radar continuously observed along the magnetic field, thereby enabling
far more independent measurements during the disturbance. The F-region
density was also greater, enabling measurements most of the time at 2j5 km.
The same two features are present at 0920 and 1210 UT, the only difference
is that they are about three times as large. The curve is dotted when
the horizontal uncertainty exceeds 50 m/s. This increase in the magnitude
with altitude is roughly what would be expected from the decrease in neutral
density. If, as we expect, the disturbances are really vertical, then the
velocities would be 24 percent of what is shown, or 30 to 40 m/s at 177 km
and 120 to 160 m/s at 235 km.

Usually these disturbances are isolated events, but on 18 January
1976, Figure 22, a case appears with three or four distinct oscillations.
The right axis shows the meridional wind velocity (neglecting a diffusion
correction of less than 10 m/s). The left axis shows the observed velocity
along the magnetic field. The impulses or wave train between 0800
and 1100 UT, if vertical, would be about the magnitude of the observed
V_{11} or 24 percent of the horizontal velocity. Again, the motion is
northward or downward. However, not all the disturbances are at night
and it is not clear whether all are northward of downward. In Figure 23
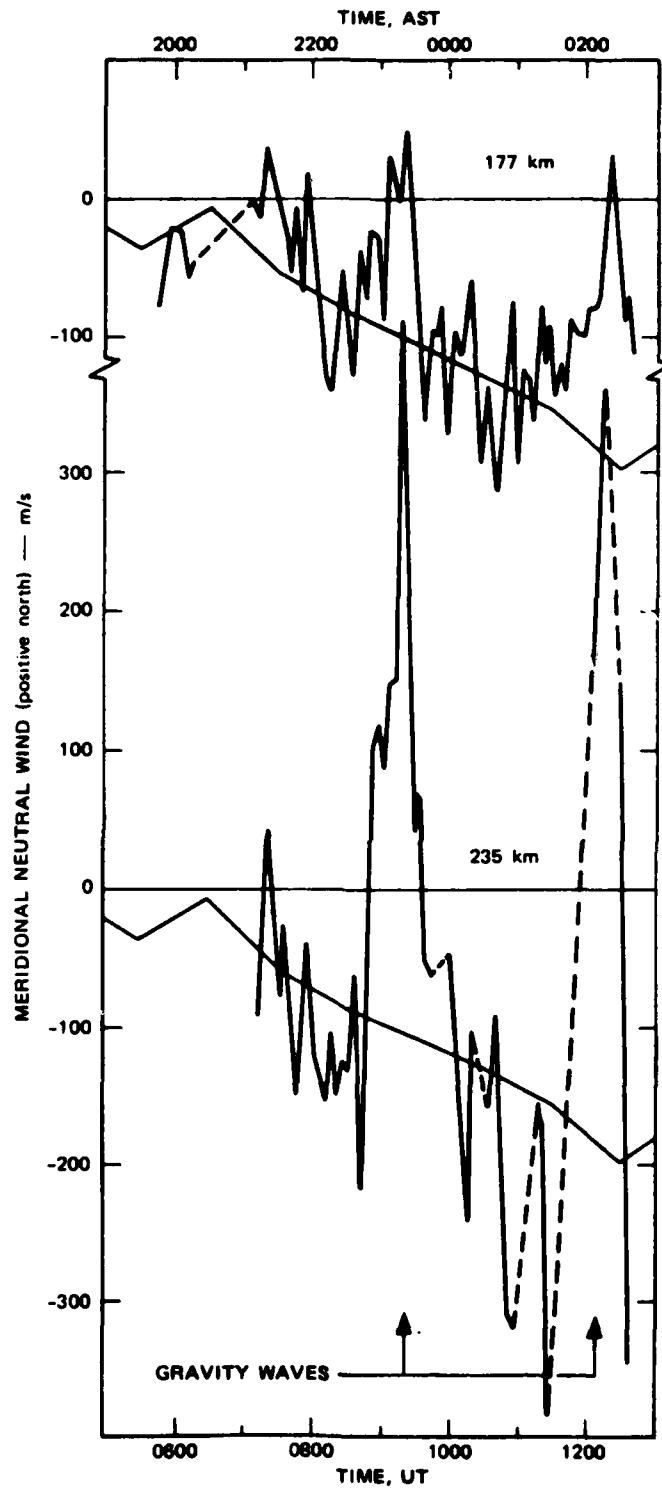
48

FIGURE 21   MERIDIONAL WIND AND GRAVITY WAVES
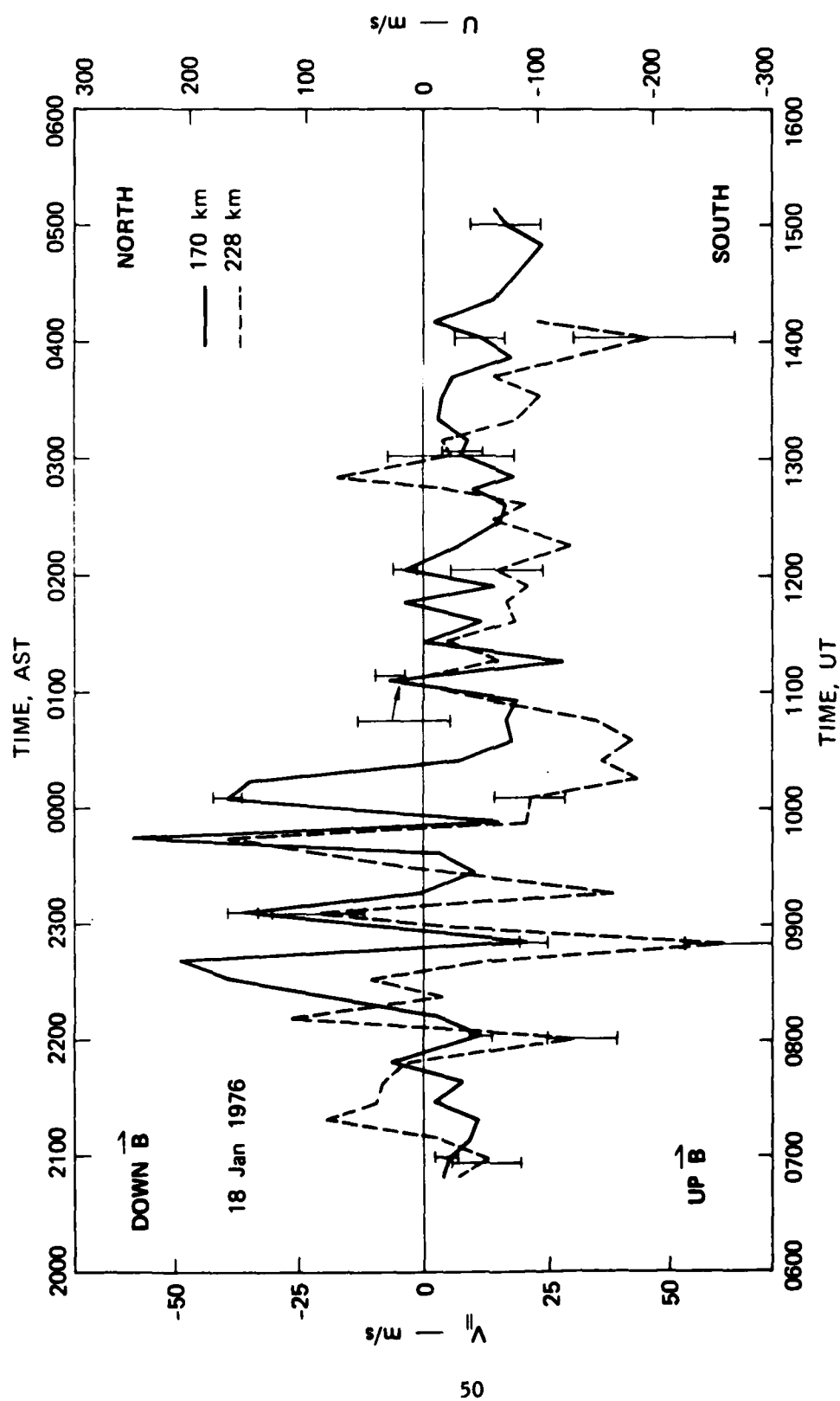DETERMINED FROM RADAR OBSERVATIONS
ON 26 FEBRUARY 1973

49

FIGURE 22   MERIDIONAL WIND AND GRAVITY WAVES DETERMINED FROM RADAR OBSERVATIONS ON
18 JANUARY 1976

50

major disturbances are centered at 2030 and 0400 UT, on either side of local noon, 18 February 1972. Again, if the impulses are vertical, as expected, then their magnitudes are 24 percent of the deduced horizontal velocity. As in the previous figures, the second one is northward or downward. The direction of the first one is difficult to determine because of the lack of data before 2000 UT to use in determining the meridional wind background. Thus, it is not clear whether the background occurs at 2000 UT near 0 m/s or at 2030 UT near 200 m/s south. If the former, then this day is not very different from the mean and the disturbance is southward or upward. If the latter, the meridional wind is extremely strong to the south, but this disturbance is in the same direction as the previous ones.

In the two incidents in Figure 23, the amplitudes are similar and they double between 168 and 227 km. Unlike the previous cases, the signal is enough to measure the disturbances near the peak of the F layer at 285 km. The amplitude of the disturbances remains the same, as at 227 km, presumably because of the influence of viscosity.

On 20 January 1972 near 1900 UT, Figure 24 shows another event similar to the first one on 18 February 1972. If the data are similar to the mean curve, then the disturbance is centered at 1900 UT and is northward or downward. If the meridional wind is near 125 m/s at 1930 UT, then the disturbance is centered at that time and is in the opposite direction. In either case, on this day, little difference exists between the amplitudes at the three altitudes.

After 2000 UT on this day, another possible wave-like disturbance with a period of about three hours and an amplitude of 100 m/s is apparent at the two higher altitudes.

In summary, a downward disturbance of one hour's duration appears in the vertical wind measured with the Fabry-Perot. In time, direction, and approximately in amplitude, these disturbances are in the simultaneous radar data. On many other occasions, large disturbances of similar duration in the meridional winds are found in the radar data. Although the radar measurements cannot distinguish directly whether these

51
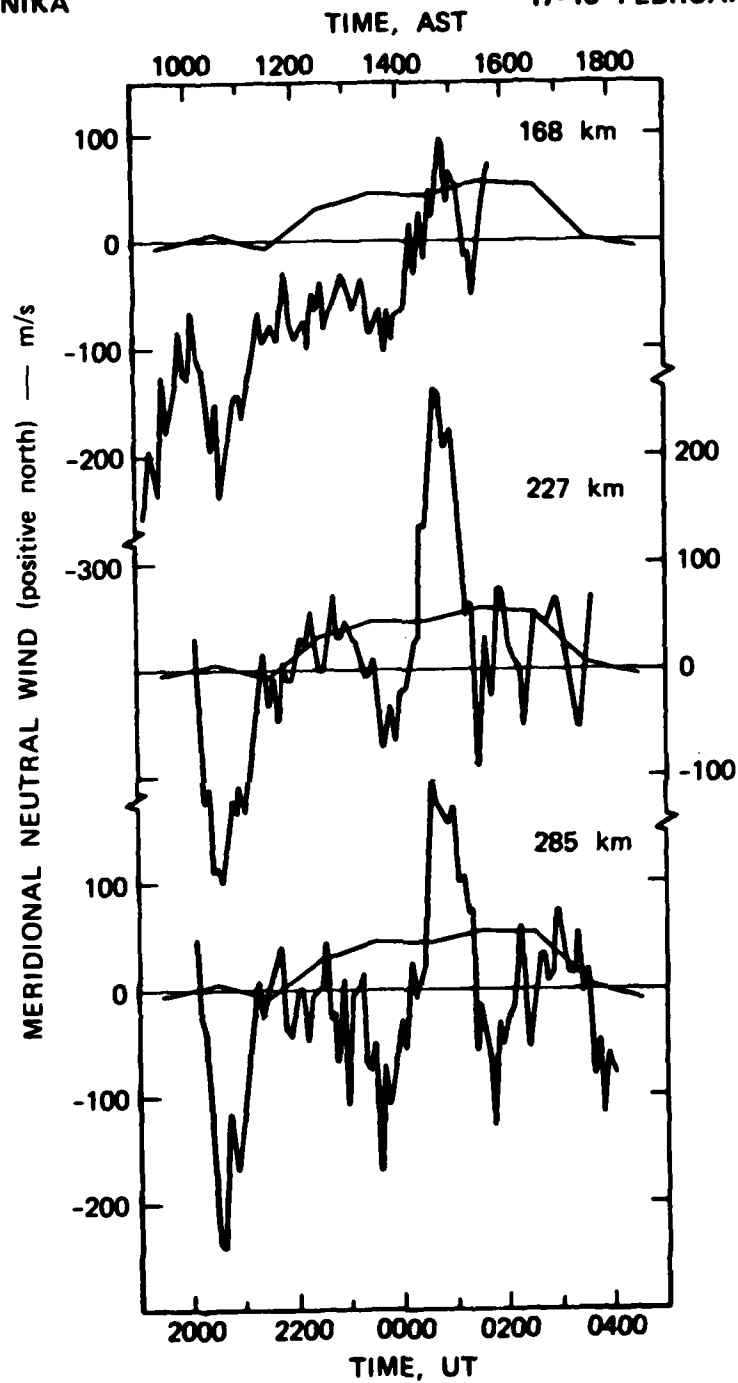
17-18 FEBRUARY 1972

FIGURE 23   MERIDIONAL WIND AND GRAVITY WAVES
DETERMINED FROM RADAR OBSERVATION
ON 17-18 FEBRUARY 1972

52

CHATANIKA   20-21 JANUARY 1972
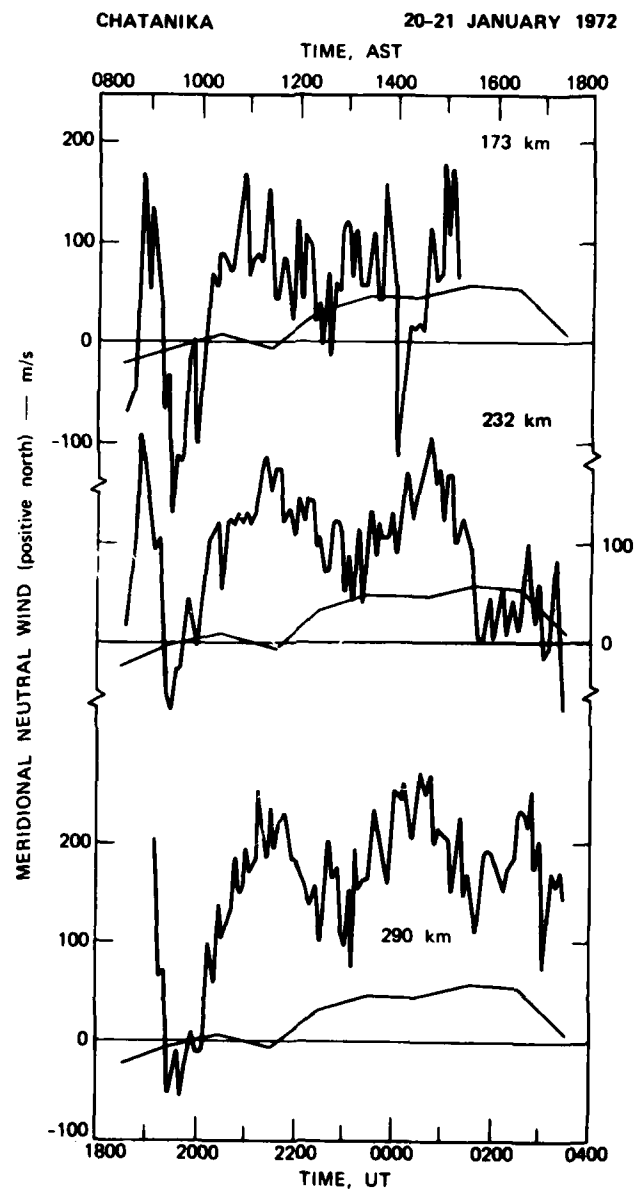
FIGURE 24   MERIDIONAL WIND AND GRAVITY WAVES
             DETERMINED FROM RADAR OBSERVATIONS
             ON 20 JANUARY 1972

53

disturbances are horizontal or vertical, they can provide strong indirect evidence that the disturbances are vertical or at least have a large vertical component. First, we can extrapolate from the agreement between the 1 March 1973 correlative data. Second, we can compare the pattern of the disturbance--characterized by the amplitude, duration, and rate of velocity change--to the Fabry-Perot meridional and vertical data. If we interpret the radar disturbance as meridional, we find no match to the Fabry-Perot meridional data in Section IV. But, if we interpret it as vertical, we find a match to the Fabry-Perot vertical data. Third, or perhaps two-and-a-half, the averaged Fabry-Perot meridional winds and averaged radar meridional winds only agree when we eliminate the large disturbances from the radar data before averaging. Or, equivalently, we do not deduce any 200- to 400-m/s variations in the meridional wind determined from the Fabry-Perot, which at an elevation angle of 30° is comparatively insensitive to vertical winds. Continuing with the radar data alone, we show that these disturbances can appear, on occasion, periodic and that they can occur during the day as well as the night. Furthermore, they usually grow in amplitude between 170 and 225 km, but not significantly between 225 and 280 km.

Our tentative interpretation of these disturbances is that they are large-scale or medium-scale gravity waves. The period suggests the large-scale gravity wave predicted by Richmond and Matsushita [1975]. These observations also appear to confirm the satellite observations of Spencer et al. [1976]. However, such an interpretation implies certain variations in density and temperature that we have been unable to examine, largely because these quantities varied during the measurements owing to particle precitation and Joule heating.

Because many of the conclusions obtained here rest on very few correlative data points and on indirect arguments, more correlative experiments should be performed in the future to confirm these conclusions. Assuming that the conclusions are correct, the next questions involve the source of these gravity waves and their properties.

VI ZONAL WIND

So far our study of the auroral-region dynamics has involved neutral motion in the magnetic meridian and vertical motion. Examination of the zonal motion is also instructive. While the meridional motion is dominated by solar EUV heating and high-latitude heating associated with auroral phenomena, the zonal motion may also be affected by ion drag, the transfer of momentum from ions to neutrals. The theoretical literature contains considerable discussion of this possibility, but the data related to this problem have been very meager. They have consisted of evidence from satellite accelerometers [DeVries, 1972] showing the existence of strong zonal neutral winds in the auroral region, from several barium-cloud releases [Meriwether et al., 1973], and from an initial comparison between the Chatanika radar and the Michigan Auroral Observatory Fabry-Perot interferometer [Nagy et al., 1974]. Thus, the data base for the examination of the role of ion-neutral drag is very limited. This data base can be substantially increased and more can be learned about this component of the neutral wind from correlative measurements made with the Fabry-Perot and radar. Such measurements exist from eight nights and show a range of magnetic activity from quiet to active.

As discussed in Sections II and III, the neutral-wind determinations were made from Fabry-Perot observations of emission from atomic oxygen at 630 nm. This emission mainly comes from an altitude range between about 180 and 250 km. The observations were made at Ester Dome, Alaska, 38 km almost magnetic south of Chatanika. The velocities were determined from the Doppler shift of measurements at a 30° elevation angle made to the magnetic west or the magnetic east. Horizontal motion was assumed, but as discussed in Section V, observations at a 30° elevation angle are not very sensitive to vertical motion. The ion-velocity determinations were made with the Chatanika radar either from resolving three line-of-sight observations at a 70° elevation angle or from observations at 45° or 70°

elevation angles made to the magnetic west or the magnetic east. In the latter case, horizontal motion was assumed. Above 150 km, any ion velocities perpendicular to the magnetic field can be compared to the neutral velocities because they are essentially constant. Thus, the neutral wind and ion velocity measurements at a given moment were separated by between 200 and 600 km, depending on the relative orientation of the two instruments. These separations were not usually important because the ion drifts and neutral winds were found very similar in both directions except during short periods of strong auroral activity or near the Harang discontinuity.

The data were acquired between 20 February and 5 April 1973 with a hole between 5 and 16 March 1973 when the moon and overcast skies interfered with the Fabry-Perot measurements. During most of the observing period, the magnetic activity was considerable, as is apparent in the distribution of data shown in Figure 7. We also show the activity for the whole period in a variety of ways in Figures 25 and 26. From the D_{st}, we see that major magnetic storms began on 21 February and 18 March. From K_p and AE, we see that large increases in the auroral region magnetic activity began with the magnetic storm and tapered slowly off during the recovery phase. From the azimuth angle, φ, of the interplanetary magnetic field (IMF), we see that the period of high magnetic activity coincided with an away sector in the solar wind. We further see large increases in the magnitude of the IMF within a day of the onset of the magnetic storm.

During this observing period we obtained good correlative data for this study on eight days. Some of these days as well as others during this period have also been used for studies of the meridional wind and vertical-velocity disturbances. One day, 22 March 1973, has previously received attention because of the large amounts of energy deposited in the atmosphere by particle precipitation and Joule heating [Wickwar, 1975].

Ion drag is a complicated phenomenon to examine because it involves the interaction of the ions and neutrals over an extended region, and the time constants are long (on the order of one hour). Indeed, attempts to model the phenomenon have involved the whole auroral region and polar cap [Knudson et al., 1977; Spiro et al., 1978; Sojka et al., 1981]. While
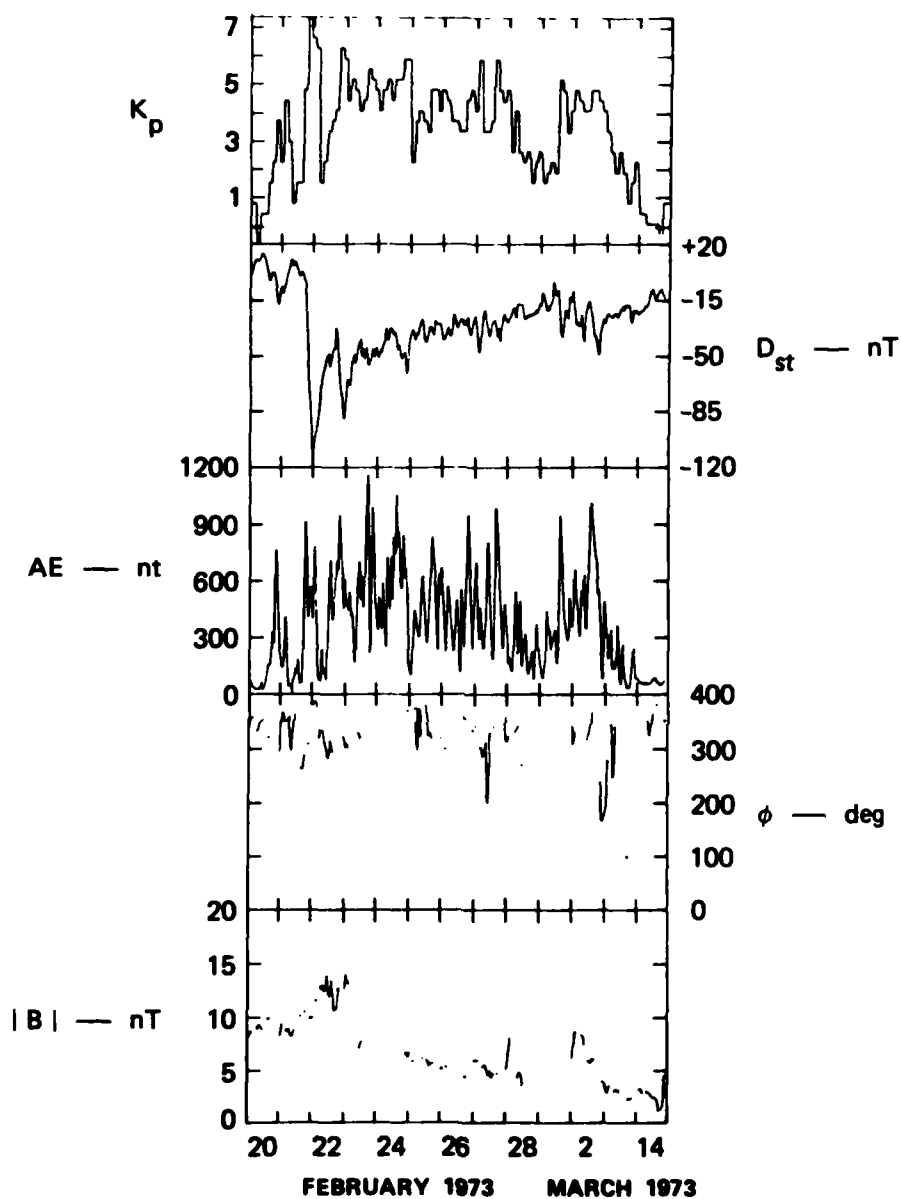
56

FIGURE 25   MAGNETIC PARAMETERS AND INTERPLANETARY-
MAGNETIC-FIELD PARAMETERS FOR PART OF THE
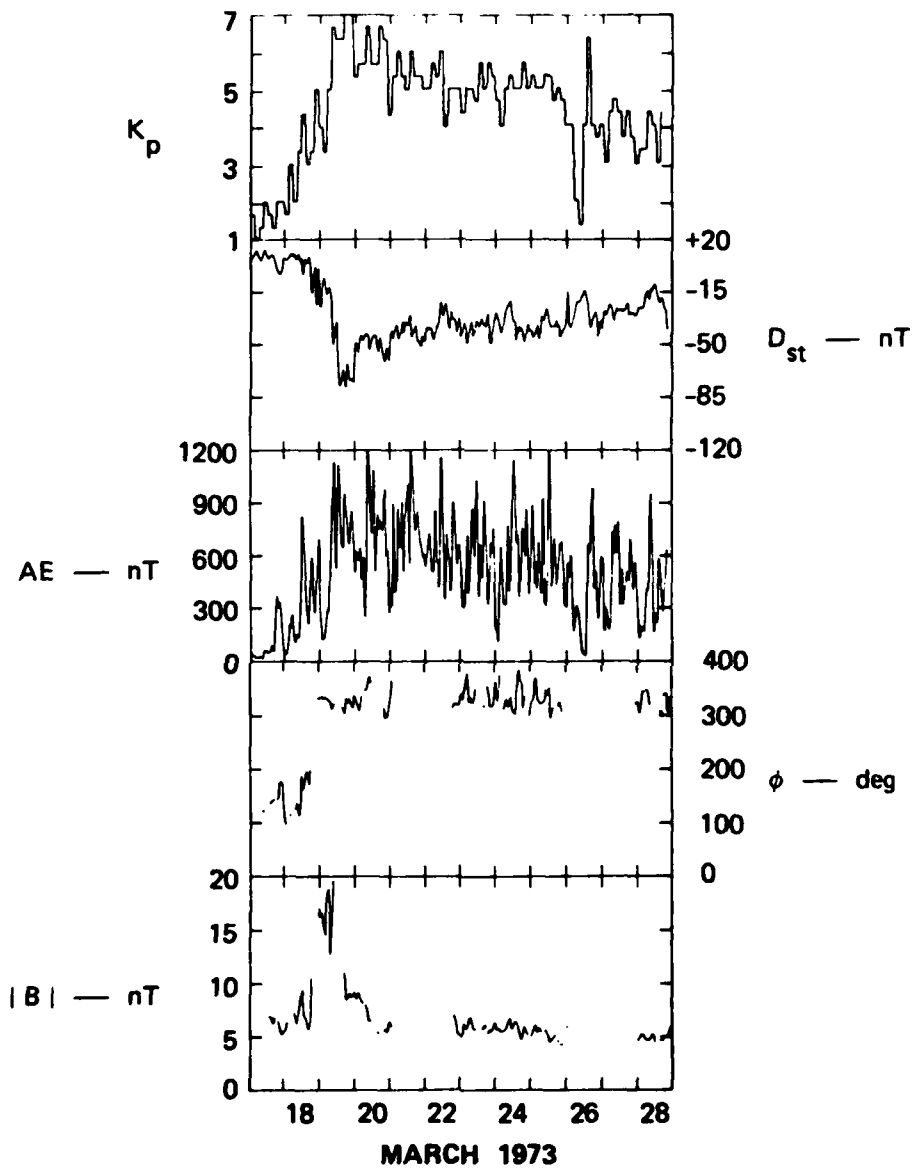PERIOD OF ZONAL-WIND OBSERVATIONS

FIGURE 26   MAGNETIC PARAMETERS AND INTERPLANETARY-
MAGNETIC-FIELD PARAMETERS FOR PART OF THE
PERIOD OF ZONAL-WIND OBSERVATIONS

58

the Fabry-Perot and radar measurements are essentially point measurements compared with the extended interaction region, they can be useful for gaining qualitative insight into this phenomena if we assume that the ionospheric conditions change slowly to the east and west. We will make the further simplifying assumption that the electron density variations at 190 km are representative of the variations between 180 and 250 km from which the 630 nm emission comes.

To gain a qualitative understanding of the processes affecting the zonal neutral wind, we will examine that wind, the east-west ion drifts, and the electron density at 190 km for the set of 8 days. In Table 3, we present the geophysical parameters describing the eight days in the order in which they are discussed.

Table 3

DATES OF EVENING SECTOR ZONAL WIND OBSERVATIONS
ALONG WITH GEOMAGNETIC- AND SOLAR-ACTIVITY PARAMETERS

Date (UT)	K_p			ΣK_p	A_p	$S_{10.7}$
	06 to 09	09 to 12	12 to 15			
4 March 1973	1	1-	1-	8+	4	96.6
27 Feb. 1973	4-	4-	4	37+	44	98.2
3 March 1973	3	2+	3	22	14	97.8
25 Feb. 1973	4+	4	4-	33	31	97.2
5 April 1973	4-	1+	1	12-	7	117.7
1 March 1973	2+	3-	2+	26+	22	99.5
23 Feb. 1973	5	4+	5-	40	48	91.4
22 March 1973	6-	5+	6	41	53	90.3

The first day to examine is 4 March 1973 (Figure 27), because it is exceedingly quiet by any standard. The whole auroral region is very quiet as indicated by K_p values between 1 and 1- during the observations. Indeed, K_p is so small that the auroral oval is likely to have shrunk such
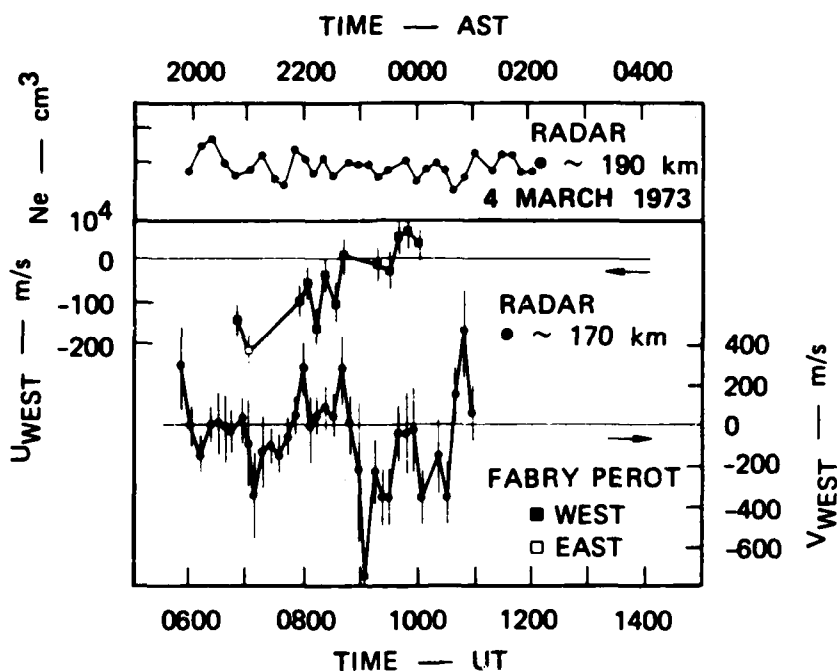
FIGURE 27   ZONAL WIND, ION DRIFT, AND ELECTRON DENSITY FOR
            4 MARCH 1973 UT

that the observations are equatorward of it [Bond and Akasofu, 1979].
Locally, the electron densities at 190 km are the lowest in this sample,
2×10^4 cm^{-3}. The zonal ion velocity is indistinguishable from zero.
The neutral wind is to the east until 0930 UT, when it turns to the west,
that is, the zonal wind is directed from day to night. This behavior is
expected theoretically [Straus, 1978; Dickinson et al., 1981] and con-
firmed by midlatitude observations [Hernandez and Roble, 1976] when the
motion is controlled by solar heating.

The other extreme occurs on 27 February 1973, Figure 28; K_p is 4-
during the observations, placing Chatanika near the center of the auroral
oval [Bond and Akasofu, 1979]. Except for the period between 0630 and
0830 UT and several other brief periods, the electron density is greater
than 7×10^4 cm^{-3}. As expected, when they result from convection electric
fields, the zonal ion velocities are large and westward before 1000 UT,
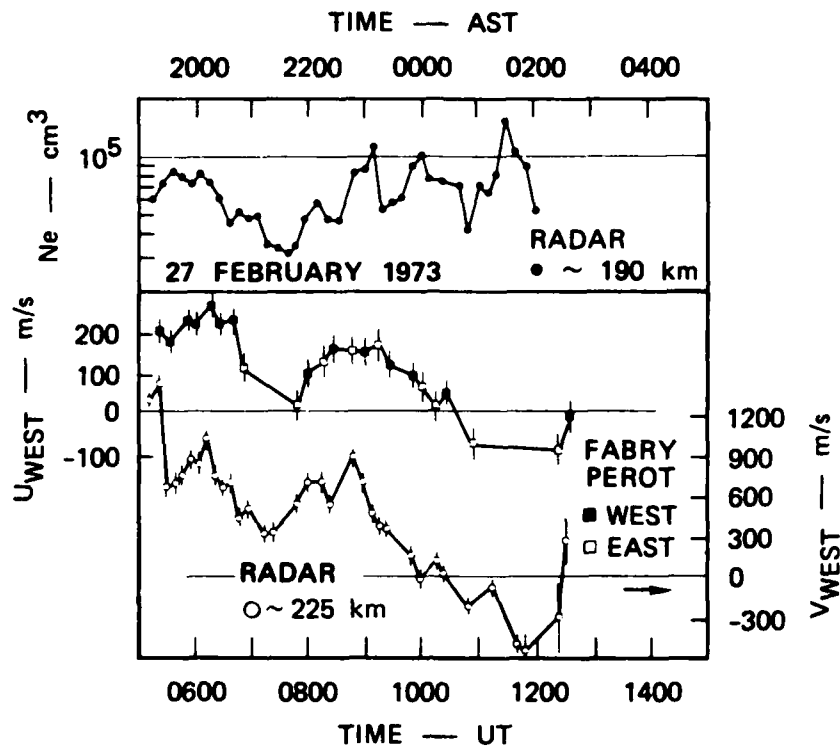and eastward thereafter until the last data point at 1230 UT. Under

FIGURE 28   ZONAL WIND, ION DRIFT, AND ELECTRON DENSITY FOR
27 FEBRUARY 1973 UT

these conditions of high electron density and large ion drifts, we find
that the zonal neutral wind does a remarkable job of tracking the ion
velocities. Thus, contrary to 4 March 1973, the neutral wind on 27 Feb-
ruary 1973 is westward in the evening and eastward in the morning.

These two days show most clearly the extremes in neutral wind be-
havior. The behavior on the first day is what we expect from pressure
gradients created by solar EUV heating. The behavior on the second day
may arise from the transfer of momentum from the ions to the neutrals or
from Joule heating that creates appropriate pressure gradients in the
neutrals. In examining the rest of our data set, we will look for corre-
lations that will enable us to address the question of which mechanism
is the more important.

Returning to the zonal winds and velocities from 27 February 1973,
we see that the neutral wind is roughly one quarter the ion drift except

61

between 0630 and 0830 UT when the electron density drops from 8×10^4 to 3×10^4 cm^{-3}.

The day that has a neutral wind behavior most like the quiet day is 3 March 1973, Figure 29. The K_p during the observations is 3 and 2+, which clearly indicates that we are within the auroral oval. The large westward ion velocities between 0630 and 0900 UT further support the auroral oval location. However, the zonal neutral wind between 0645 and 1015 UT is almost identical to that of the quiet day rather than to that of the active, i.e., to the east. Besides the neutral wind, the major distinguishing feature is that the electron densities at 190 km are closer to those of the quiet day than those of the active day, i.e., 3×10^4 rather than 8×10^4 cm^{-3}. At 0930 UT, the electron densities increase to 1×10^5 cm^{-3} and we see the neutral wind become westward by 1015 UT, a behavior much more like that of the active day.

25 February 1973, Figure 30, behaves similarly to 3 March. K_p is 4+ and 4 during the observations, values that are slightly higher than those on what we are calling the active day. The ion velocities before 0740 UT are strongly westward. Yet the zonal neutral velocities are initially eastward and then slightly westward. Again, the apparent difference is that the local electron density is low before 0740 UT, but not as low as on the quiet day or on 3 March 1973. After 0740 UT, the electron density increases to the level of the active day and the ion velocities become eastward. The neutral velocities now follow the ion velocities in that they are eastward.

5 April 1973, Figure 31, behaves still differently. K_p is 4- and 1+ during the observations. As on 25 February, 27 February, and 3 March, which have all had moderate K_p values (3 or 4) between 0600 and 0900 UT, the ion velocity is strongly westward. In agreement with 27 February, 5 April 1973 has a high electron density 1×10^5 cm^{-3} during this period, and the neutral wind is westward. Indeed, the electron density is higher and the neutral wind is more strongly westward than on 25 February. Shortly after 1100 UT, which is when the other days including the "active" day all had high electron densities, eastward ion velocities and eastward
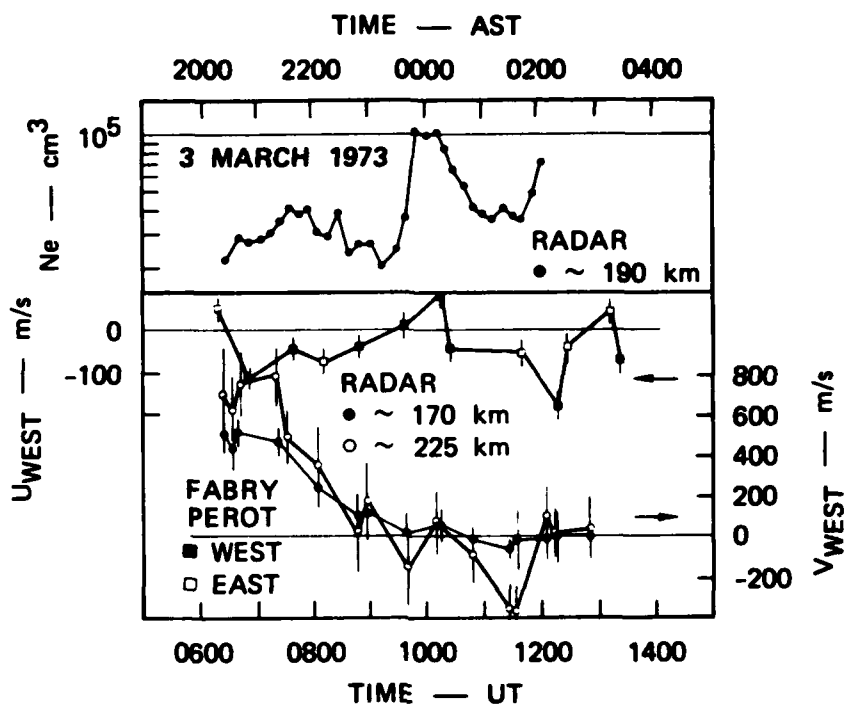
62

FIGURE 29   ZONAL WIND, ION DRIFT, AND ELECTRON DENSITY FOR 3 MARCH 1973 UT

neutral winds, this day has a drop in the electron density to 4×10^4 cm^{-3}, and the neutral wind is westward, as might be expected from solar heating [Straus, 1978].

On 1 March 1973, Figure 32, the results are similar to 25 and 27 February, although the data are much more limited. Between 1000 and 1200 UT, the K_p value is 3-, and the zonal ion velocities that change from westward to eastward are strong. The neutral wind similarly changes from westward to eastward in this period. As on the two February days, the density is high, 8×10^4 cm^{-3}.

On 23 February 1973, Figure 33, we have a very active day with K_p values of 5 and 4+ and very large electron densities, about 1.5×10^5 cm^{-3}. The neutral winds seem to vary in the same way that the ion velocities vary, initially going west, then, later east. However, following the details on this day is difficult because the data points are fewer.
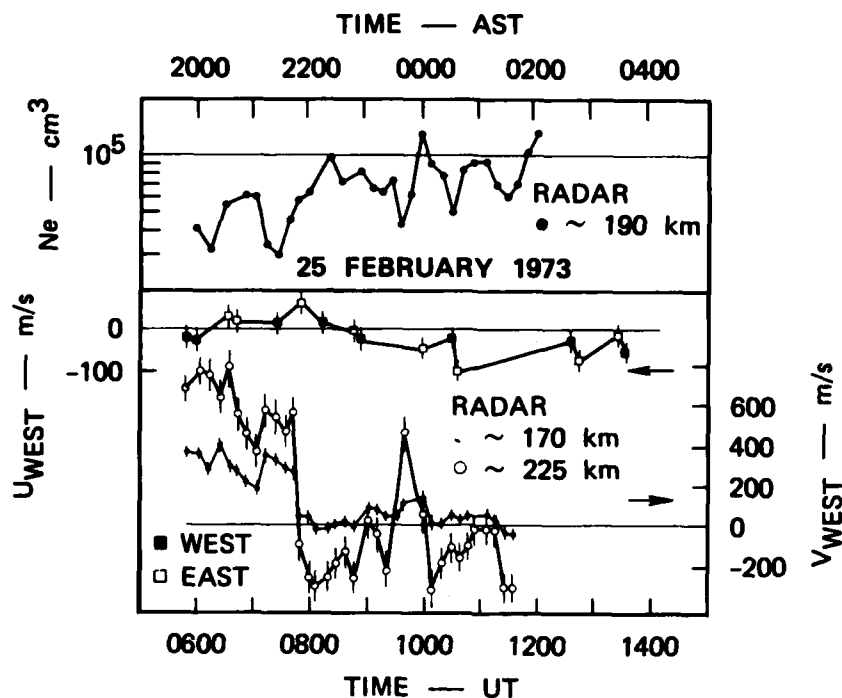
FIGURE 30   ZONAL WIND, ION DRIFT, AND ELECTRON DENSITY FOR
25 FEBRUARY 1973 UT

The last day is 22 March 1973, Figure 34. It is the most active
day with K_p values of 6- and 5+. The zonal ion velocities become zero
very early and then become very strongly eastward. Initially, the elec-
tron densities are near 2×10^5 cm^{-3} and then stay near 1×10^5 cm^{-3}.
From what we have seen so far we would expect the neutral winds to track
the ion winds. They tend to do so, but appear to be offset to the west.
However, this relationship, which has occurred for all the previous data,
breaks down significantly between 1140 and 1240 UT when the ion velocities
approach 1 km/s eastward. The neutrals remain westward, but with a lower
velocity.

The important question is whether we can find common elements in the
correlative observations on these eight nights. The first point is that,
when we are equatorward of the auroral oval as on 4 March 1973, we have
qualitative agreement between the zonal neutral wind and theoretical
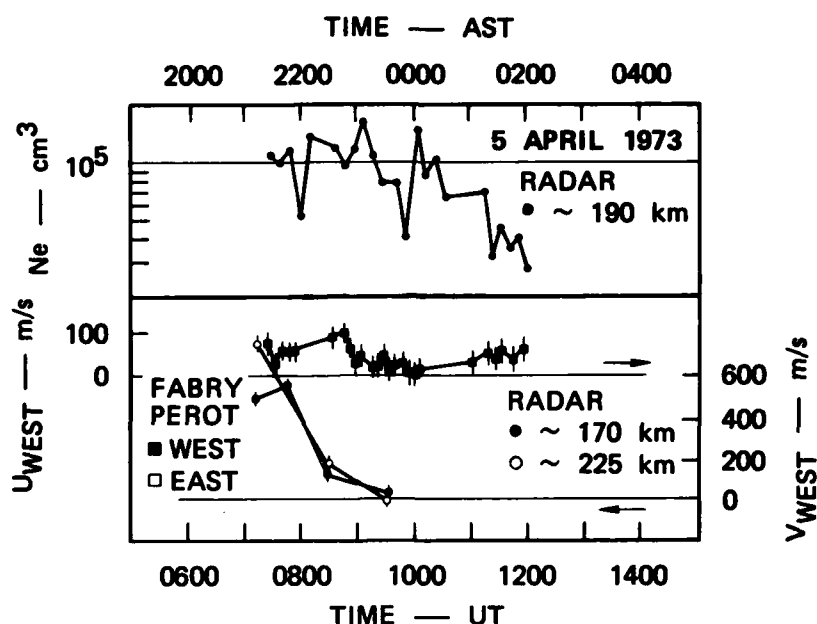
64

FIGURE 31   ZONAL WIND, ION DRIFT, AND ELECTRON DENSITY FOR
5 APRIL 1973 UT

values derived from solar EUV energy input.   The second point is that,
when we are in the auroral oval, and ion convection velocities are strong,
the neutrals are affected to a greater degree as the local electron density
is increased.   For densities near 2×10^4 cm^{-3}, there is little effect.
For densities near 1×10^5 cm^{-3}, the neutrals move as though closely
coupled to the ions.   This coupling, provided by the local electron den-
sity, is consistent with ion drag being an important factor in the neutral
equation of motion.   The argument that ion drag is the important term
here can be strengthened by noting that the forces on the neutrals are
away from the Harang discontinuity, i.e., from the region where the zonal
ion velocity changes direction.   Joule heating cannot account for this
force because it would have to be located at the discontinuity, precisely
where the ion velocity, hence electric field, is small or zero.   The third
point is that, on the most active day, 22 March 1973, Joule heating also
becomes important.   Between 0800 and 1130 UT, the neutral wind tracks the
ion velocity as usual, with an additional westward component that becomes
bigger as we approach the period from 1140 to 1240 UT.   This occurs when

65
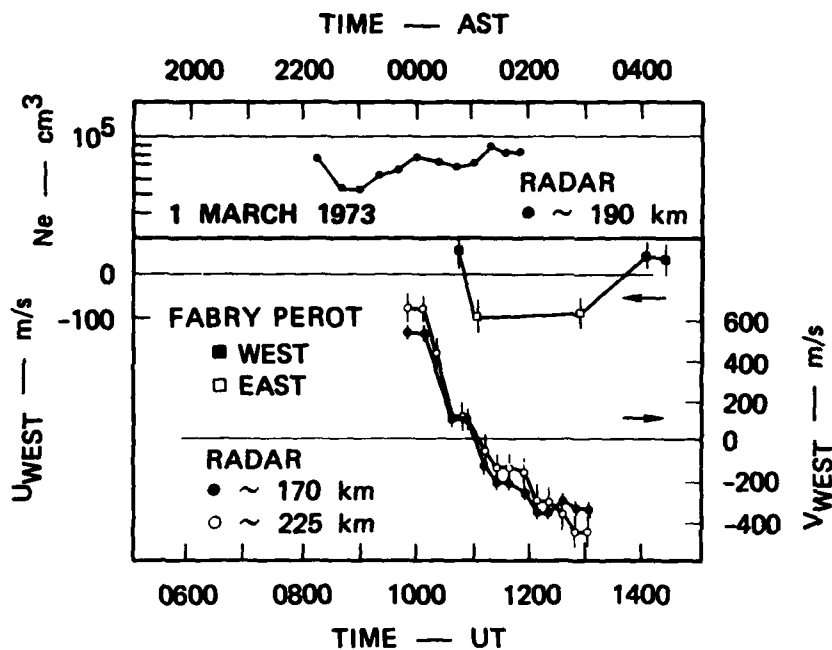
FIGURE 32   ZONAL WIND, ION DRIFT, AND ELECTRON DENSITY FOR
1 MARCH 1973 UT

the Joule heating event [Wickwar, 1975] is very large, roughly 25 ergs/cm^2-s, leading to a 400°K ion temperature increase in the F region and upper portions of the E region. It is as though the Joule-heated region had been in existence for several hours and Chatanika had been rotating toward it. The fourth point is that, based on the number of occurrences in this small sample, ion drag appears to be a more important neutral force term in the equatorward portion of the auroral oval than Joule heating.

FIGURE 33   ZONAL WIND, ION DRIFT, AND ELECTRON DENSITY FOR
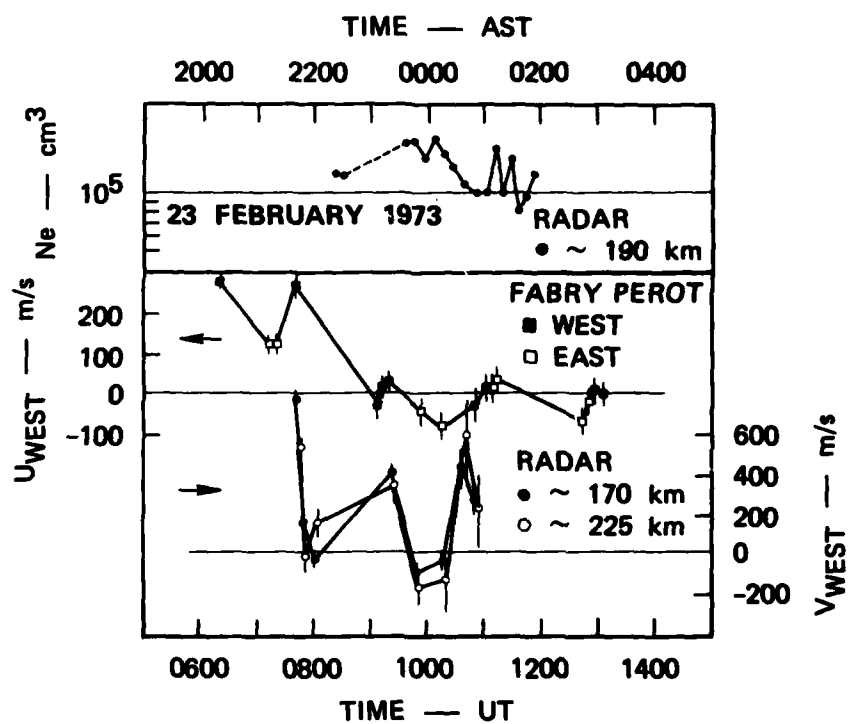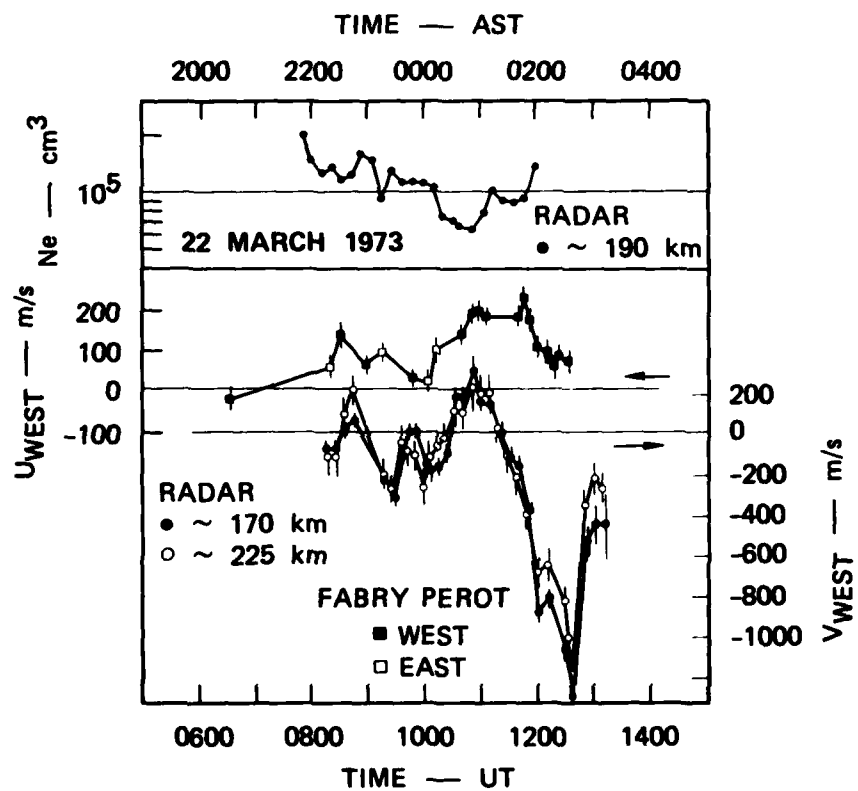23 FEBRUARY 1973 UT

67

FIGURE 34   ZONAL WIND, ION DRIFT, AND ELECTRON DENSITY FOR
22 MARCH 1973 UT

VII E-REGION WIND

The E region is a much more difficult region in which to make wind measurements than the F region because the wind varies substantially with altitude. The experimental procedure is different, involving a multiple pulse rather than a single long pulse. The technique is described by Rino et al., [1974]. The distinction between methods and the application to wind measurements are discussed by Rino et al. [1977]. In practice the multiple-pulse technique has been used for observations at Chatanika since March 1978. The system used for these measurements is described in Kofman and Wickwar [1980].

The analysis procedure is also considerably more involved. Initial indications of what can be accomplished were presented in Rino et al. [1977]. Since then, progress in combining all the simultaneous measurements has been made so that, by late 1979, the long-pulse measurements were used to determine the electric field much more accurately and the short-pulse measurements were used to determine the electron densities. Both these quantities, as shown in Section II, are needed in addition to the ion-velocity measurements. The uncertainties in the multiple-pulse velocity measurements first became available in mid-1980 with the installation of ACFIT, a program that determines velocities and temperatures by means of a nonlinear least squares fit of theoretical autocorrelation functions to the measured autocorrelation functions. A good summary of the current status of the analysis software is provided by de la Beaujardiere et al. [1980], and an example of ACFIT applied to E-region temperatures is given by Wickwar et al. [1981].

Despite the significant improvements in observing and data reduction that have occurred since the Rino et al. [1977] paper, further improvements are required in data reduction before an extensive analysis of the data acquired since March 1978 is warranted. These include (1) interpolation of data from each of three line-of-sight positions to a single time before

69

resolving the vector ion velocity; (2) derivation of the vector neutral
velocity, not just the components perpendicular to the magnetic field;
and (3) propagation of errors from the line-of-sight velocities to the
components of the vector velocities. The first will reduce errors intro-
duced into the data by temporal and spatial variations in the electron
fields and neutral winds. The second will enable finding the horizontal
north-south velocity and the vertical velocity for the first time. The
third will, of course, enable determining when the measurements are
significant. Most of the developmental work for these improvements has
been accomplished.

While we were improving our analysis techniques, we also made several
attempts to analyze portions of the data to see if we were on the right
track. The first attempts at determining E-region velocities over long
periods of time produced long-term sinusoidal variations that are very
similar to those seen at lower latitudes and interpreted as tidal motion.
Hence, an examination of the data for tidal components and auroral per-
turbations seems worthwhile.

VIII SUMMARY

In summary, at F-region altitudes, we compared winds measured with the radar with those measured with the Fabry-Perot and have verified our technique for determining meridional winds. We found (1) large vertical velocities that are probably gravity waves, (2) an average meridional wind and variations about it caused by magnetic activity, as well as (3) suggestions of seasonal variation. We also found considerable day-to-day variations and an altitude gradient, at least between 175 and 225 km. In the zonal component, we examined the day-to-day variations and found many times when the wind was strongly affected by ion drag, and one period when Joule heating also had to have been present. In the E region, we have improved the analysis procedure to the point where examination of the body of data that is accumulating is justified.

REFERENCES

Banks, P. M., and G. Kockarts, _Aeronomy_ (Academic Press, New York, 1973).

Bond, F. R., and S.-I. Akasofu, "Comparison of Auroral Ovals from All-Sky
    Camera Studies and from Satellite Photographs," _Planet. Space Sci._,
    _27_, 541-549 (1979).

Chandra, S., D. Krankowsky, P. Lämmerzahl, and N. W. Spencer, "Auroral
    Origin of Medium-Scale Gravity Waves in Neutral Composition and
    Temperature," _J. Geophys. Res._, _84_, 1891-1897 (1979).

Cogger, L. L., G. J. Nelson, M. A. Biondi, R. D. Hake, Jr., and D. P.
    Sipler, "Coincident F-Region Temperature Determinations from Inco-
    herent Backscatter and Doppler Broadening of (OI) 6300A;" _J. Geophys._
    Res., _75_, 4887-4889 (1970).

Cogger, L. L., J.C.G. Walker, J. W. Meriwether, and R. G. Burnside, "F-
    Region Airglow: Are Ground-Based Observations Consistent with Recent
    Satellite Results?" _J. Geophys. Res._, _85_, 3013-3020 (1980).

Davis, M. J., and A. V. Da Rosa, "Traveling Ionospheric Disturbances Ori-
    ginating in the Auroral Oval during Polar Substorms," _J. Geophys. Res._,
    _74_, 5721-5735 (1969).

De la Beaujardière, O., V. B. Wickwar, C. Leger, M. McCready, and M. J.
    Baron, "The Software System for the Chatanika Incoherent-Scatter
    Radar," Technical Report, SRI Project 8358, SRI International, Menlo
    Park, CA (1980).

DeVries, L. L., "Structure and Motion of the Thermosphere Shown by Density
    Data from the Low-G Accelerometer Calibration System (OGACS)," _Space_
    Res., _12_, 867-879 (1972).

Dickinson, R. E., E. C. Ridley, and R. G. Roble, "A Three-Dimensional
    General Circulation Model of the Thermosphere," _J. Geophys. Res._, _86_,
    1499-1512 (1981).

Evans, D. S., N. C. Maynard, J. Trøim, T. Jacobsen, and A. Egeland, "Auro-
    ral Vector Electric Field and Particle Comparisons, 2. Electrodyna-
    mics of an Arc," _J. Geophys. Res._, _81_, 2235-2249 (1977).

Evans, J. V., "Incoherent-Scatter Contributions to Studies of the Dynamics
    of the Lower Thermosphere, _Rev. Geophys. and Sp. Phys._, _16_, 195-216
    (1978).

Forbes, J. M., and H. B. Garrett, "Theoretical Studies of Atmospheric Tides," Rev. Geophys Sp Phys., 17, 1951-1981 (1979).

Hays, P. B., and R. G. Roble, "Direct Observations of Thermospheric Winds During Geomagnetic Storms," J. Geophys. Res., 76, 5316-5321 (1971).

Hays, P. B., R. A. Jones, and M. H. Rees, "Auroral Heating and the Composition of the Neutral Atmosphere," Planet. Sp. Sci., 21, 559-573 (1973).

Hays, P. B. J. W. Meriwether, and R. G. Roble, "Nighttime Thermospheric Winds at High Latitudes," J. Geophys. Res., 84, 1905-1913 (1979).

Hays, P. B., A. F. Nagy, K. D. McWatters, and J. V. Evans, "Comparison of Radar and Optical Temperature Measurements in the F Region," J. Geophys. Res., 75, 4881-4882 (1970).

Hernandez, G., and R. G. Roble, "Direct Measurements of Nighttime Thermospheric Winds and Temperatures, 1. Seasonal Variations During Geomagnetic Quiet Periods," J. Geophys. Res., 81, 2065-2074 (1976).

Jacchia, L. G., "Revised Static Models of the Thermosphere and Exosphere with Empirical Temperature Profiles," Smithsonian Astrophysical Observatory, Cambridge, Special Report 332 (1971).

Kelly, J. D., and V. B. Wickwar, "Radar Measurements of High-Latitude Ion Composition Between 140 and 300 km," J. Geophys. Res., 86, 7617-7626 (1981).

Kofman, W., and V. B. Wickwar, "Plasma-Line Measurements at Chatanika with High-Speed Correlator and Filter Bank," J. Geophys. Res., 85, 2998-3012 (1980).

Knudsen, W. C., P. M. Banks, J. D. Cunningham, and D. M. Klumpar, "Numerical Model of the Convecting F_2 Ionosphere at High Latitudes," J. Geophys. Res., 82, 4784-4792 (1977).

Meriwether, J. W., Jr., P. B. Hays, K. D. McWatters, and A. F. Nagy, "Doppler-Shift Measurements of Weak Spectral Emissions with a Large Aperture Fabry-Perot Interferometer," Technical Report, Space Physics Research Laboratory, University of Michigan, Ann Arbor, MI (1975).

Meriwether, J. W., Jr., J. P. Heppner, J. D. Stolarik, and E. M. Wescott, "Neutral Winds Above 200 km at High Latitudes," J. Geophys. Res., 78, 6643-6661 (1973).

Nagy, A. F., R. J. Cicerone, P. B. Hays, K. D. McWatters, J. W. Meriwether, A. E. Belon, and C. L. Rino, "Simultaneous Measurement of Ion and Neutral Motions by Radar and Optical Techniques," Radio Sci., 9, 315-321 (1974).

Olson, W. P., and K. Moe, "Influence of Precipitating Charged Particles on the High-Latitude Thermosphere," J. Atmos. Terr. Phys., 36, 1715-1726 (1974).

Rees, M. H., A. I. Stewart, and J.C.G. Walker, "Secondary Electrons in Aurora," Planet. Space Sci., 17, 1997-2008 (1969).

Richmond, A. D., and S. Matsushita, "Thermospheric Response to a Magnetic Substorm," J. Geophys. Res., 80, 2839-2850 (1975).

Rino, C. L., A. Brekke, and M. J. Baron, "High-Resolution Auroral-Zone E-Region Neutral Wind and Current Measurements by Incoherent Scatter Radar," J. Geophys. Res., 82, 2295-2304 (1977).

Rino, C. L., M. J. Baron, G. H. Burch, and O. De la Beaujardière, "A Multipulse Correlator Design for Incoherent-Scatter Radar," Radio Sci., 9, 1117-1127 (1974).

Roble, R. G., and M. H. Rees, "Time Dependent Studies of the Aurora: Effects of Particle Precipitation on the Dynamic Morphology of Ionospheric and Atmospheric Properties," Planet. Sp. Sci., 25, 991-1010 (1977).

Schunk, R. W., and J.C.G. Walker, "Theoretical Ion Densities in the Lower Ionosphere," Planet. Sp. Sci., 21, 1875-1896 (1973).

Sojka, J. J., W. J. Raitt, and R. W. Schunk, "A Theoretical Study of the High-Latitude Winter F Region at Solar Minimum for Low Magnetic Activity," J. Geophys. Res., 86, 609-621 (1981).

Spencer, N. W., R. F. Theis, L. E. Wharton, and G. R. Carignan, "Local Vertical Motions and Kinetic Temperature from AE-C as Evidence for Aurora-Induced Gravity Waves," Geophys. Res. Lett., 3, 313-316 (1976).

Spiro, R. W., R. A. Heelis, and W. B. Hanson, "Ion Convection and the Formation of the Mid-Latitude F-Region Ionization Trough," J. Geophys. Res., 83, 4255-4264 (1978).

Straus, J. M., "Dynamics of the Thermosphere at High Latitudes," Rev. Geophys. Sp. Phys., 16, 183-194 (1978).

Swider, W., and R. S. Narcissi, "Auroral E-Region: Ion Composition and Nitric Oxide," Planet. Sp. Sci., 25, 103-116 (1977).

Testud, J., "Gravity Waves Generated During Magnetic Substorms," J. Atmos. and Terr. Physics, 32, 1793-1805 (1970).

Wickwar, V. B., "Chatanika Radar Measurements," Atmosphere of Earth and the Planets, B. M. McCormac, ed., (D. Reidel Publishing Co., Dordrecht, Holland, 1975).

Wickwar, V. B., L. L. Cogger, and H. C. Carlson, "The 6300Å O(^{1}D) Airglow and Dissociative Recombination," _Planet. Sp. Sci._, _22_, 709-724 (1974).

Wickwar, V. B., C. Lathuillere, W. Kofman, and G. Lejeune, "Elevated Electron Temperatures in the Auroral E Layer Measured with the Chatanika Radar," _J. Geophys. Res._, _86_, 4721-4730 (1981).